FACULTY
OF MATHEMATICS
AND PHYSICS
Charles University

BACHELOR THESIS

Lucia Kapitánová

Cosmic ray study in the Belle II silicon detector

Institute of Particle and Nuclear Physics

Supervisor of the bachelor thesis: doc. RNDr. Zdeněk Doležal, Dr.

Study programme: Physics

Specialization: General Physics

Prague 2019

I declare that I carried out this bachelor thesis independently, and only with the cited sources, literature and other professional sources.

I understand that my work relates to the rights and obligations under the Act No. 121/2000 Coll., the Copyright Act, as amended, in particular the fact that the Charles University has the right to conclude a license agreement on the use of this work as a school work pursuant to Section 60 paragraph 1 of the Copyright Act.

In…..... date..... signature

I would like thank my supervisor, doc.Zdeněk Doležal, for his valuable insights in the field of high energy physics, my parents for their support, and most importantly I would like to thank my thesis consultant, Mgr. Jakub Kandra, for his assistance and countless advice without whose help this work would not have been possible.

Title: Cosmic ray study in the Belle II silicon detector

Author: Lucia Kapitánová

Department / Institute: Institute of Particle and Nuclear Physics
Supervisor of the bachelor thesis: doc. RNDr. Zdeněk Doležal, Dr., Institute of Particle and Nuclear Physics

Abstract: This thesis introduces validation and monitoring tools developed and adjusted for the Belle II vertex detector used during the VXD commissioning run in October and November of 2018. The introductory review part introduces the Belle II detector and provides detailed description of the vertex silicon detector, its components and their functions. Subsequently, the software reconstruction methods are introduced and the applied alignment procedure is explained in the third section. The major focus of this thesis is presentation of validation and monitoring results as well as qualitative description of the measurement precision improvement using cosmic muons trajectories reconstructed in the vertex detector. The last part introduces a new tool for estimation of alignment parameters using monitoring and validation methods. The main purpose of this newly proposed method is to provide fast and credible information about the current alignment status to experts using this data.

Keywords: Silicon detector, Cosmic rays, Belle II experiment

Contents

Introduction

The Standard model (SM) belongs among the most successful experimentally tested and verified theories of all times. However, despite its undoubtable predictive power, leading to numerous Nobel Prizes, the SM comes with many questions and puzzles yet to be answered.

One of the most successful approaches, proposed to reveal its secrets, has proven to be the symmetry study. A closer study of symmetries and their fundamental origins has already enlightened many dark areas of scientific interest. This approach has been tested in many different fields of Physics among which one is of particular importance for this thesis - the matter-antimatter asymmetry of the universe from cosmological scale [1] [2]. Experiments indicate that a study of CP symmetry breaking is the right track to follow in order to find out more about this topic.

Two different approaches are currently being taken in order to zoom in at the symmetry-breaking origin. The energy frontier approach, being the main area of interest for experiments such as ATLAS and CMS, and the approach at the rare/precision frontier, represented by the B-physics experiments [1].

So-called „B factories“ mostly focus on B meson decay channels and observation of CP asymmetry between $\overline{B}^0 \rightarrow J/\psi K^0_S$ and $B^0 \rightarrow J/\psi K^0_S$. In order to be able to observe and study these processes, the detecting facility and technique must meet quite demanding requirements, including extremely high luminosity (beam intensity), very precise spatial resolution and event vertex reconstruction as well as reliable particle identification [1] [3].

There were two B-physics facilities successful at supporting Cabibbo-Kobayashi-Maskawa (CKM) model, a theory explananing the CP asymmetry. These were the Belle experiment at the Japanese KEKB facility and the BaBar experiment at SLAC. Both were designed to collide e^-e^+ particle beams at the center of mass energy corresponding to the rest mass of $\Upsilon(4S)$ particle [1]. Sufficient luminosity reached at KEKB allowed for measurements precise enough to confirm the theoretical predictions of the Standard Model and bring the Kobayashi-Maskawa Nobel Prize of 2008.

However, luminosity itself would not suffice for a successful discovery. When using the time dependent CP-asymmetry method in B-meson decay studies,

reconstruction of the interaction point (IP) is crucial. Successful decay vertex reconstruction asks for a very precise position measurements. [1] Precision achieved solely by mechanical installation of the device is insufficient and further verification and monitoring of accuracy is required.

Monitoring can be carried out with help of well studied and understood physical processes, for example, by closer analysis of expected and measured trajectories of a particle passing through the detector volume. With no magnetic field present in the detector, this examination can help improve the accuracy and precision of trajectory reconstruction as well as combine information obtained from different parts of the detector [1] [3]. Tracks of cosmic particles have been used for this purpose in numerous experiments. Following parts of this thesis deal with a specific application of this method to the upgraded Belle II detector.

The first chapter of the thesis introduces the Belle II detector and provides brief information about its components. The second chapter in detail focuses on the vertex part of the detector. The tools used for data processing and information reconstruction are described in the third chapter. The fourth chapter introduces the topic of the most interest for this thesis – the alignment procedure and its implementation for the Belle II experiment. The final chapters provide overview and discussion of author's findings and results of the alignment procedure validation and quality monitoring performed by author using cosmic ray data.

1 The Belle II detector

As a successor to the Belle detector, which successfully achieved all of its technological and scientific goals set back in the 20th century, comes its upgrade, the Belle II detector.

Operation plan for Belle II picks up directly where the Belle experiment left off. The main goal of this detector is to continue the study of CP violation in B-meson decays by precise measurement of its decay channels.

Just like its predecessor, the Belle II detector operates at the asymmetric electron positron collider, this time, however, of a Super B factory upgrade of the Belle's KEKB collider – SuperKEKB [1][2].

This new generation collider, designed to reach 40 times larger luminosity than KEKB, has laid its eye on producing roughly about 50 ab^{-1} collisions. The "precision" frontier of nowadays heavy flavor physics experiments searching for evidence of New Physics can undoubtedly benefit from such high luminosity. Nevertheless, it does not come without consequences. As a result of luminosity induced increased beam background, the new collider is more technically demanding. The upgrade of the detector was, therefore, inevitable [3].

SuperKEKB is a double ring collider, with respective beam energies of 7 GeV for the high energy ring (HER) of electrons and 4 GeV for low energy ring (LER) of positrons. The experiment uses nano-beam large crossing angle collision scheme [1][3].

Electrons for the HER ring are produced by a photo-cathode RF gun while large emmittance positron beam is created by a flux concentrator [1]. Because of the short lifetime of positrons in LER low emmitance of positrons is required. This leads to a need for an addition of a positron damping ring.

Once a collision occurs, products of the event, originating from the interaction point, penetrate further into the active volume of the detector and pass through its individual layers. The Belle II detector is mostly composed of upgraded Belle sub-detectors with several new innovative components (Figure 1.1).

Closest to the beam pipe, the vertex detection system, in comparison with the Belle's silicon vertex detector enhanced by two additional innermost layers of silicon pixel detector, is found.

The vertex detector together with the central drift chamber (CDC) form the tracking system of the Belle II detector. The CDC, surrounding the vertex detection system, measures particle's momentum based on curvature of its trajectory in the local magnetic field. The measured average energy loss in the CDC volume, filled with a mixture of gasses, provides a helpful information for the process of particle identification.

This process is mostly done by the particle identification system (PID) based on results of Cherenkov radiation measurements, which are carried out in the TOP and ARICH detectors located at the barrel and endcap parts of the detector respectively. The PID system uses data obtained from CDC and VXD detector components to separate long lived kaons and pions. These are, together with muons, subsequently detected by the KLM system, separated from the PID device by the electromagnetic calorimeter (ECL). The main task of ECL is to measure the energy of charged and gamma particles passing through its volume [1][2].

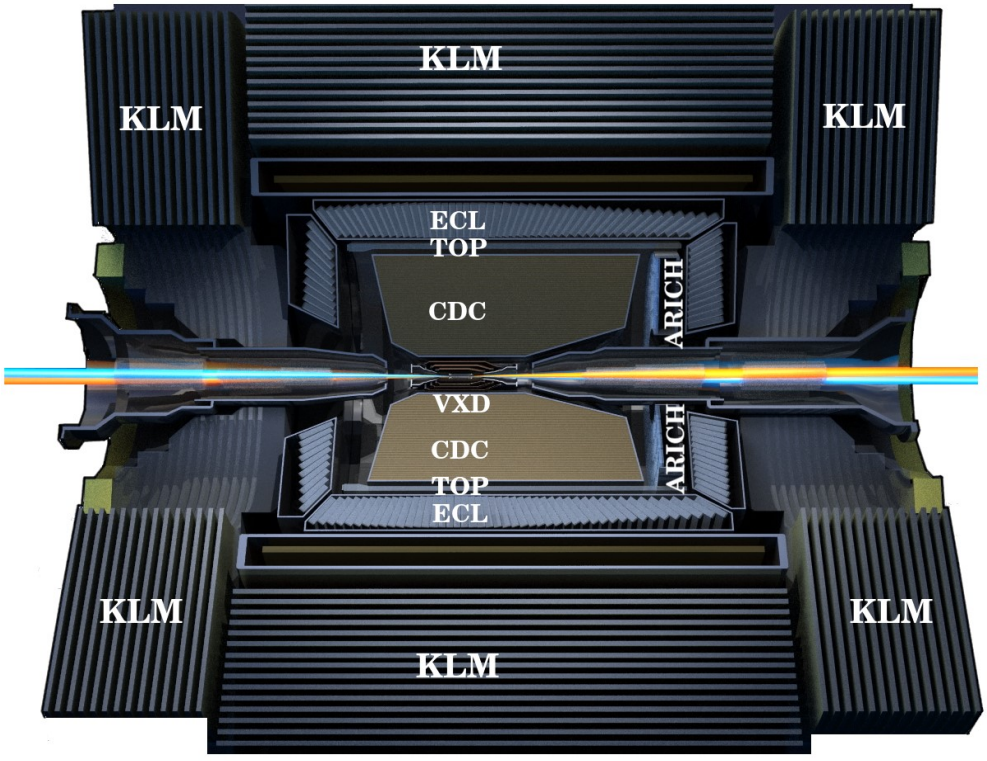

Figure 1.1: Belle II detector cross section [4]

2 Vertex Detector

The most significant novelty introduced in Belle II, in demand for high special resolution, excellent hit reconstruction ability, good resistance to radiation and low material budget, is the innermost part of the detector comprised of two layers of active silicon pixel detecting system (PXD).

This new system has to be able to cope with the substantially increased background resulting from being located closest to the beam pipe and collisions. Moreover, thanks to a full silicon construction no additional support of the measuring system is needed, which makes the depleted p-channel field effect transistor (DEPFET) technology the most auspicious candidate meeting all the proposed requirements. This technology, applied to each pixel, combines detection and in-pixel amplification [5].

The pixel detecting system is surrounded by several layers of strip vertex detector (SVD) sensors. The ability of SVD to reconstruct tracks with p_T as low as several tens of MeV/c is very valuable, especially in D* decay products studies [1]. The SVD part of the detector has to satisfy slightly different set of conditions including fast read-out, mechanical durability and operation dependability.

Strip vertex detector (SVD) and pixel vertex detector (PXD) combined together create a unit called **the vertex detector** that is about to be referred to as the VXD in the rest of this work.

2.1 Pixel Vertex Detector – PXD

Two layers of active pixel sensor are located as close to the beam pipe as possible, only 14 mm from the interaction point.

Each pixel cell of DEPFET system includes a field effect transistor implemented on a fully depleted n-type bulk [6]. An electron-hole pair, created by a charged particle in the volume of a pixel cell, gets separated and the created signal electrons drift towards the surface of the cell, while the holes progress in direction of

the p-contact thanks to the presence of internal electric field. A potential minimum is created by deep n-doping implantation underneath the main transistor's gate forming a so called „internal gate" where the signal electrons, created by a particle traversing through the substrate, are being collected. Charge cumulated in the inner gate then proportionally modulates the current between the source and the drain of the field effect transistor [5]. The readout of the obtained information itself does not influence collected charge. Therefore, a clear (n+) contact is in charge of emptying the collected electrons from the gate by applying additional positive pulse. Other cells are turned off during the readout process. Figure 2.1 shows a cross sketch of a DEPFET sensor layout.

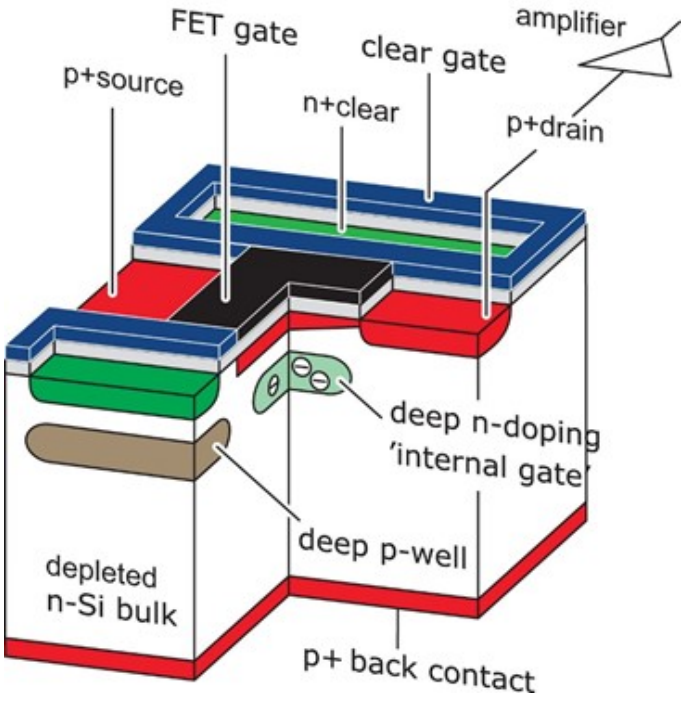

Figure 2.1 DEPFET pixel sensor [6]

Sensitive area of sensors in the first layer is 2.5 × 44.8 mm^2. The outer region of the first layer is formed by sensors 50 × 60 μm^2 in size and the dimensions of sensors in the central region are 50 × 55 μm^2. Sensors in the second layer are slightly bigger, with the corresponding sensitive area size 12.5 × 61.44 mm^2. The pixel sizes of the sensors in the outer and the central regions of the second layer are 50 × 85 μm^2 and 50 × 70 μm^2 correspondingly [7].

2.2 Strip Vertex Detector (SVD)

The innermost pixel layers of the vertex detector are surrounded by four layers of silicon strip detectors organized into ladders, forming a windmill structure, the numbering of which is explained and described in Figure 2.5.
The strip vertex detector (SVD) not only provides additional information about B-meson decays, in addition to data obtained from the inner PXD detector, but also detects other decay channels occurring past the PXD volume by measuring the energy of the incident particle deposited in individual strip.

The SVD part of the detector consists of 172 n-type high resistivity bulk sensors with the width of approximately 320 μm. Double-sided strip detectors (DSSD) are implemented in the whole SVD structure. Two coordinate tracking information is obtained thanks to the mutual orthogonality of strips on both sides of a sensor (Figure 2.2).

A passing charged particle generates electron-hole pairs in the active part of the sensor. The created negative charge-carriers are collected by N^+ strips while holes are being recorded by P^+ strips [1].

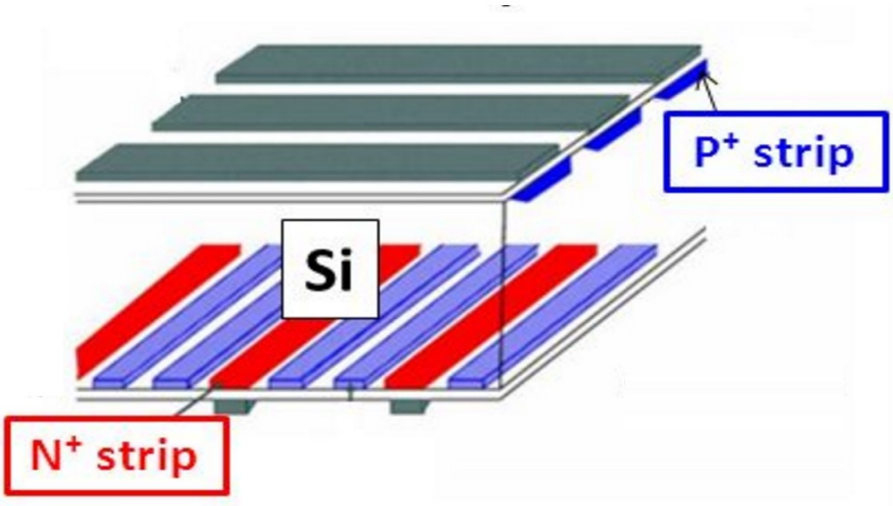

Figure 2.2: DSSD strip sensor [1]

Two different shapes of strip sensors are used in different parts of the detector – rectangular and trapezoidal. The central barrel part is formed by rectangular sensors. Their size varies depending on the layer number. Four layers lay successively at the 38, 80, 115 and 140 mm distance from the interaction point [3].

Sensors in the barrel part of each layer are implemented parallel to the z-axis (consistent with the beam pipe direction). The front part of the detector, facing forward in respect to the boosted particles in the beam pipe, requires slanted trapezoidal sensors covered by strips which are no longer perfectly aligned with the z-axis [1] [3] [7].

The outwards facing side of strips, denoted as "n-side", located along the r-θ coordinate lines, correspond to the shorter side of the strip.

The first layer of strip detector sensors, the subsequent sensor layer surrounding the PXD part, possesses sensitive area of 38.4 × 122.8 mm^2 with p-pitch (p-side referring to the longer r-θ side of the slanted sensors) 50 μm and n-pitch 160 μm at z-side. The parallel sensors in all remaining layers of the SVD part have the sensitive area of 57.6 × 122.8 mm^2 with a corresponding p-pitch 75 μm and n-pitch 240 μm. Similar values apply to the slanted sensors size which differ by their spatial orientation. Trapezoidal wedged sensors possess sensitive area of 38.4 - 57.6 × 122.8 mm^2 with p-pitch 50 – 75 μm and n-pitch 240 μm [7].

This configuration allows for a full coverage of Belle II angular acceptance spanning between $17^\circ < \theta < 150^\circ$.

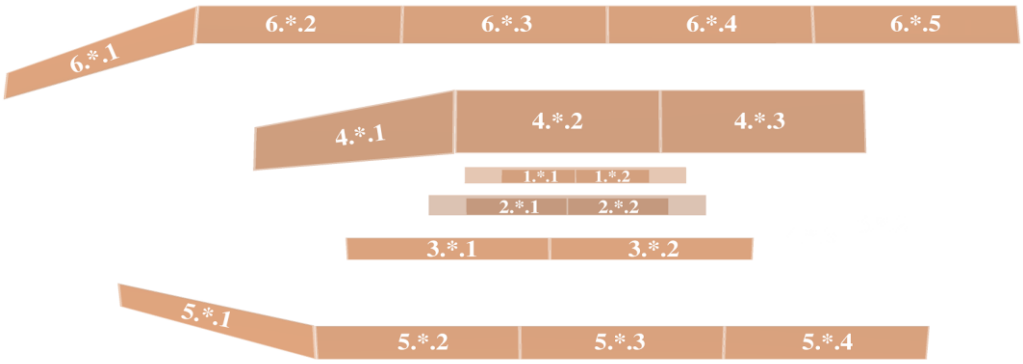

Figure 2.3: Numbering of sensors in ladders – the first number in notation refers to layer, the last number denotes the ladder number and stars (*) in center represent ladder number in layers [7]

Figure 2.3 shows that ladders in the 6th layer are formed by 5 sensors, ladders in layers 5 a 4 consist of 4 and 3 sensors correspondingly. The innermost 3 layers of

the vertex detector are composed of 2 sensors each. Numbering of sensors in each ladder explained in detail in Figure 2.5.

2.3 VXD Commissioning

In Summer of 2018, two halfshells of strip detector were successfully assembled. The proper opertion of hardware, readout system, reconstruction and tracking software was tested. The parallel pixel detector was commissioned in Europe and then transported to KEK. In October 2018, the vertex part of the detector was successfully constructed and assembled (Figure 2.4).

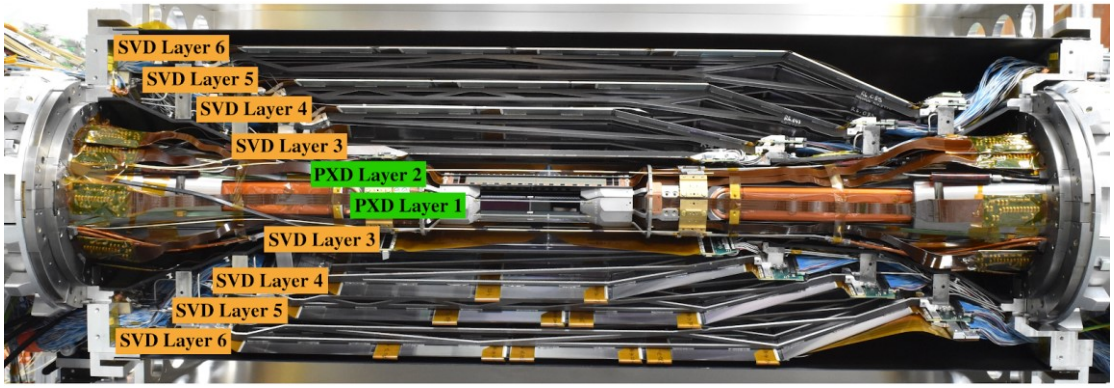

Figure 2.4: Vertex detector after final assembly pixel and strip detector [8]

At the current setup stage, the vertex detector is still missing one half of the pixel sensors. The final setup of VXD ladders can be seen in Figure 2.5. The second layer is designed to contain 12 ladders comprised of 2 sensors each. However, only two ladders, 2.4 and 2.5, with 2 sensors per ladder are currently being used for data collection. [8]

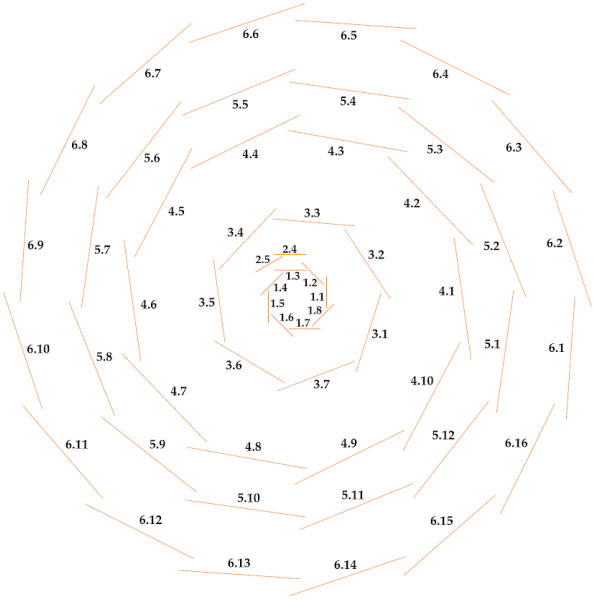

Figure 2.5: Numbering of ladders in corresponding layers for VXD Commissioning – the first number in notation refers to layer while the second number denotes the ladder number [7].

2.4 Trigger setup

Triggers are a very important component of detecting apparatus. Trigger systems are in charge of data selection taking into account the computing power limitations of the used technology. In order for the data analysis to focus only on the relevant events, their main task is to sort out only events interesting for the particular experiment. So as to achieve the highest possible efficiency, many different ways and decision making criteria are being applied. [9]

For commissioning of the Belle II vertex detector, plastic scintillators were used. Scintillator panels were placed around the VXD part, fully covering the area of its active parts. For the functionality testing of the VXD detector before its final installation, trigger logic was based on coincidence of events between oppositely oriented scintillators was used. During the cosmic data taking, events detected by both opposing scintillators were looked for in the data recorded by the detector.

The trigger setup is explained in Figure 2.6.

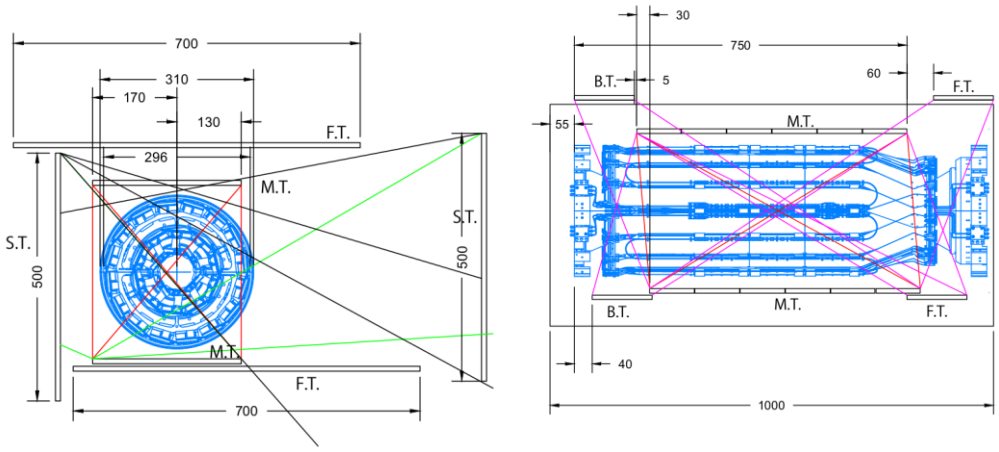

Figure 2.6: Trigger setup around vertex detector during commissioning run. Both cross (left) and longitudinal (right) views show top, bottom parts (F.T., B.T. and M.T.) of trigger and side part (S.T.) of trigger. [8]

2.5 Data Acquisition System

Coincidence observed by the trigger starts off a procedure of transportation and processing of the detected information. Figure 2.7 explains the logical sequence of steps in the procedure of information transportation from PXD / SVD sensors to servers used for data storing. The recorded datasets are labelled with experiment number and numbers of corresponding runs within which the data was collected. After the data collecting run, the detected information was stored at DAQ Storage 5 (Figure 2.7) and copied to KEKCC server where it was analyzed. [8]

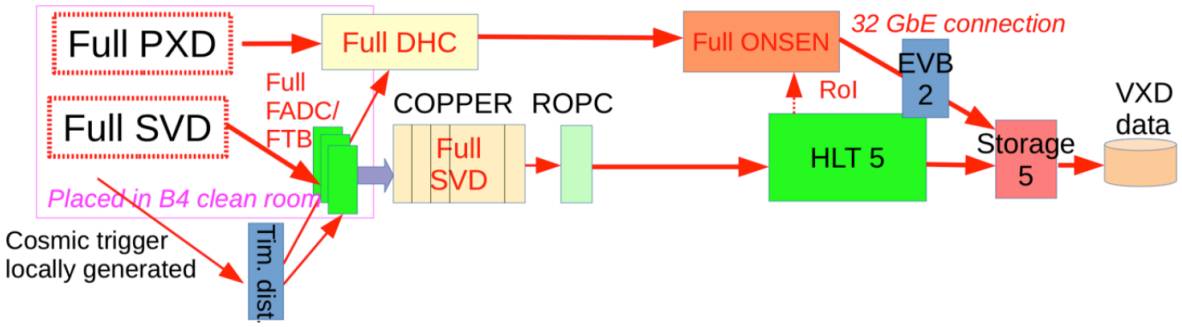

Figure 2.7: Data acquisition system for VXD Commissioning [8]

3 Belle II analysis and software framework

Software tools are inevitable links between the measurement and data analysis.

Data collected by a sensor are passed down to a software tool to be processed and interpreted. Sensor measures current position of a passing charged particle. The position information is then handed over to an analysis software tool, the task of which is to translate analogous signal into digital form. The transformed information is delivered in a computer-readable form.

The obtained raw data first get unpacked by a digitizer and turned into "digit"–like information. Each strip is assigned a value which marks strips containing information valuable for further analysis. Second module, a so-called clusterizer, groups up these "digit"–tagged strips in order to reconstruct full position information called a hit. An SVD cluster, containing 1D information about the location of each hit, as well deposited charge information, is created. Two mutually perpendicular clusters need to be combined in order to fully reconstruct a hit on an SVD sensor: one on the *u* side and one on the *v* side of the sensor. Measurements made by the PXD sensor of the vertex detector undergo a similar analysis resulting in PXD clusters. However, unlike SVD clusters, a PXD cluster already contains 2D information about hit position.

The next step combines SVD and PXD clusters information together in order to select out hits located on the same track. However, this track finding process is done in global coordinate system, while the hit information is obtained in local coordinates of the given sensor. The procedure of transformation in between these frames of reference makes use of alignment parameters to be discussed in the following chapter. A constraint of minimum of 3 hits on a track is imposed on the track finding process. Redundant information is forgotten. The result of the track finding procedure is a container of reconstructed tracks, called RecoTracks. Reconstructed track contains sorted elements of selected analyzed clusters. In the last step of the procedure, a reconstructed track is fitted and two new classes called "Track" and "TrackFitResult" are created [8].

When a charged particle passes through a magnetic field, it is being acted upon by a force which makes it deviate from its otherwise linear trajectory. In a general case, considering the particle's velocity being non-parallel to the magnetic field, this force

results in a helical motion of the particle. [10] Parametrization of such a particle trajectory by a helix with 5 parameters is a commonly used fitting technique in high energy physics. However, in our special case with no magnetic field present, only three parameters of the fit are relevant. The resulting data arrays contain information about number of hits per track.

4 Alignment

The path of a charged particle can be traced and reconstructed using the signal it created in active volume of detector components. As described in Chapter 2, charged particles deposit energy and create electron-hole pairs when traversing pixel or strip sensors of the vertex detector. This signal gets transformed into spatial position information – a hit. A series of such hits, associated with signals created by the same particle, form the particle path – a track. Hits, corresponding to particle's current position, are measured in local coordinate systems of detecting sensors with relatively small uncertainties (several microns when assuming perfect planarity of a sensor) [1] [11].

The track fitting procedure, connecting hits that belong to the same trajectory, uses hit measurement information and relative positions of detecting sensors. Mutual position of sensors is, initially, before the alignment procedure, estimated from the geometry scheme of the detector. Mechanical assembly of the apparatus and surface deformations of installed sensors are possible sources of substantial uncertainties.

If the relative position of sensors based on the construction plan and their surface planarity do not coincide with reality, track parameters and fitted trajectories are considerably biased. This discrepancy between nominal positions and real detector geometry leads to erroneous interaction vertices reconstruction, particle identification and invariant mass calculation [11].

Detection of sensor position deviations from their nominal values and their surface deformations is the main task of a process called alignment. The alignment procedure calculates real sensor spatial position and minimizes tracking bias.

The result of alignment is a set of alignment parameters. These parameters are applied to initial position values and these corrected values are used for future fitting. Corrections applied to relative sensor positions allow for realistic and more accurate fitting results.

The process of alignment discussed in this work is focused on application of general alignment procedure on the vertex part of the Belle II detector.

Sensor positions determined from detector geometry design are not precise enough to meet the requirements of time-dependent CP violation measurements [1]. Identification of b-quarks and analysis of other processes involved in studies of matter-

antimatter asymmetry ask for precision better than 10 μm [for further details see Belle II design report or B-factories book – [2]].

As previously stated, detector initial geometry can be influenced by mechanical assembly and additional manipulation with its subcomponents. The apparatus is also a subject to natural phenomena including earthquakes and changes of ambient pressure and humidity. That yields that its geometry evolves in time.

Because of these conditions, alignment corrections to initial positions should be determined quickly and, as a precaution, repeatedly during data taking. With the use of modern software alignment tools and online or offline–alignment validation procedure we are able to achieve maximum result precision and accuracy of physical measurement.

4.1 Track based alignment

The main goal of the alignment procedure is to determine rigid body (6 parameters per sensor) and surface deformation corrections (at least 3 parameters per sensor). A very large number of free parameters needs to be determined. (see Table 4.1).

One of the possible methods of acquiring precise sensor position is a method of track based alignment. This procedure focuses on minimization of the difference between expected and measured trajectory hits. So as to avoid biased output parameter combinations and increase tracking precision, the procedure uses large number of topologically rich track sets. Biased paramameter combination would correspond to a geometrical configuration of detector satisfying the trajectory fit (in agreement with the alignment parameter values), however not corresponding to a realistic arrangement. Therefore the alignment process also imposes logical physical constraints on estimates of parameters corresponding to system's degrees of freedom [1].

	Layer	*Radius* [mm]	*Ladders*	*Sensors per ladder*	*Sensors*	*Alignment parameters* *Rigid*	*Surface*
PXD	1	14	8	2	16	96	48
PXD	2	22	2	2	4	24	12
SVD	3	39	7	2	14	84	42
SVD	4	80	10	3	30	180	90
SVD	5	104	12	4	48	288	144
SVD	6	135	16	5	80	480	240
Total			65		192	1152	576

Table 4.1: Summary table for vertex detector

Results of fitting procedure need a quality evalution method able to represent agreement between the measured hit positions and fitted particle trajectory. Quantitative difference between the two can be expressed by a normalized residual.

Normalized residual, representing deviation z_{ij} of a measured recorded hit i associated with the *j-th* track u_{ij}^{m} from its expected model-based value u_{ij}^{p}, is given by a formula [1] [3]:

$$z_{ij} = \frac{u_{ij}^{m} - u_{ij}^{p}(\boldsymbol{\tau}_j, \boldsymbol{a})}{\sigma_{ij}} = \frac{r_{ij}(\boldsymbol{\tau}_j, \boldsymbol{a})}{\sigma_{ij}} \tag{1}$$

The normalization parameter σ_{ij} stands for measurement uncertainty. The residual value as well as the predicted hit coordinate are multivariable functions of fitted track parameters $\boldsymbol{\tau_j}$ and global alignment parameters $\boldsymbol{\alpha}$. The smaller the residual value, the better the track to hit agreement is reached.

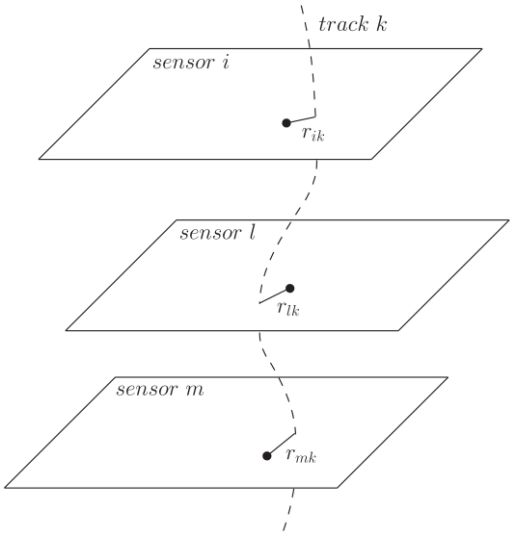

Figure 4.1: Illustration of connecting sensors using tracks and definition of track-to-hit residuals. [8]

4.2 Determination of alignment parameters using Millepede II

The quality of reconstructed track can be very well illustrated by χ^2 function. Chi-squared distribution is a commonly used evaluation method for determination of quality of a fit. This function is mathematically expressed by sums of normalized residuals over all tracks and corresponding hits.

The functional dependance on small corrections ($\delta\boldsymbol{\tau}$) of the initial local geometry parameter values ($\delta\boldsymbol{\tau_0}$) and corrections ($\delta\boldsymbol{\alpha}$) of initial alignment parameters ($\delta\boldsymbol{\alpha_0}$) is, in estimation, expanded to a linear order.

The Belle II alignment procedure uses Millepede II Algorithm specifically designed for exact calculation of alignment parameters based on linearised minimisation of residuals with possibility of further constraints imposition [1] [3] :

$$\chi^2(\tau, a) = \sum_j^{tracks} \sum_i^{hits} z_{ij}^2(\tau_j, a) \simeq$$
$$\sum_j^{tracks} \sum_i^{hits} \frac{1}{\sigma_{ij}^2} (r_{ij}(\tau_j^0, a^0) + \frac{\partial r_{ij}}{\partial a} \delta a + \frac{\partial r_{ij}}{\partial \tau_j} \delta\tau_j)^2 \quad (2)$$

Quality of reconstructed track is indirectly proportional to value of the χ^2 function. Small function values correspond to too good agreement between fitted and real passing particle trajectory. Global minimal value of the function corresponds to a perfectly aligned detector [11][12].

Every sensor and track included in the measurement analysis is being treated individually and gets assigned corresponding set of coordinates and fitting parameters respectively. Sensors and tracks are parameterized in two different sets of coordinates. The local frame of reference with origin positioned in the center of a sensor (marked $r_0=(x_0,y_0,z_0)$ in global coordinate system) uses local set of coordinates denoted *u,v* and *w,* corresponding to a general vector notated $q=(u,v,w)$. W is the coordinate orthogonal to the plane of a sensor while the *u* and *v* axis are parallel to the sides of a sensor. Global coordinates represent the laboratory system with a general vector defined as $r=(x,y,z)$.

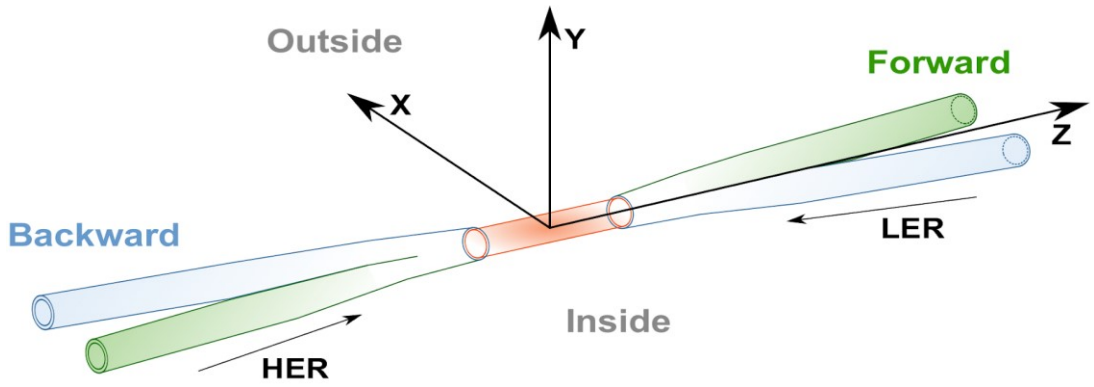

Figure 4.2: The global set of coordinates common for the entire experiment [7]

Transformation from global to local coordinate system is easily done in algebraic representation [1]:

$$r = RT\Delta R(q + \Delta q) + r_0 \tag{3}$$

where R represents a rotation matrix corresponding to transformation from global to local coordinate system. Because of uncertainties in rotations and shifts along the axis infinitesimal corrections are applied. The ΔR matrix is a product of three infinitesimal rotations by angles $\Delta\alpha$, $\Delta\beta$ and $\Delta\gamma$ around three local coordinate axis. Incremental shift in general direction is marked by the $\Delta q = (\Delta u, \Delta v, \Delta w)$ vector. The rotations and shifts can be understood from the Figure 4.3.

When working with Millepede II software, method of General Broken Lines (GBL) is used frequently. GBL method allows the algorithm to account for multiple scattering effects during the alignment parameters calculation. GBL uses a 2-thin scatterer approximation of material distribution in the detecting volume affecting the direction and general attributes of charged particle's propagation [1] [13].

4.3 Alignment parametrization

Set of alignment parameters $\boldsymbol{a}$ (in equation (2)) of a planar sensor that need to be determined by the alignment procedure is composed of these components: rigid body ($\Delta u, \Delta v, \Delta w, \Delta\alpha, \Delta\beta, \Delta\gamma$) and surface deformation parameters.

The rigid body parameters (Figure 4.3) are three parameters used for description of sensor's relative movement and three parameters for relative rotations around the coordinate axes. The rigid body parameters are defined as corrections applied during

the transformation of extrapolated hit position from global to local sensor coordinate system. The standard labels of alignment parameters are *u, v* and *w* for shifts of sensors and *α, β* and *γ* for rotations of sensors around the axes of shifts.

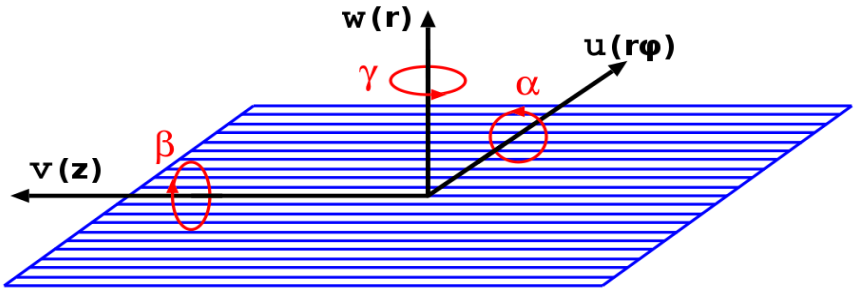

Figure 4.3: Rigid body parameters in local coordinate system of sensor: Axis *u* pointing in direction of the shorter side of sensor with associated rotation angle *α,* axis *v* parallel to the longer side of sensor with associated angle *β* and axis *w* in direction perpendicular to the sensor plane with rotation angle *γ*. All local coordinates show relative direction in global coordinate system. [7]

Surface deformations of sensors can be described by deformation parameters (Figure 4.4) characterizing the projection of measured quantities to the perpendicular direction *w(u,v).* Parametrization based on Legendre polynomials was used. The two-dimensional description can be obtained by combining one-dimensional Legendre polynomials corresponding to both directions of measurement. One of the perks of working with Legendre polynomials (denoted by L_i) is their orthogonality, which can be expressed mathematically as follows :

$$x \in [-1,1] \qquad \int_{-1}^{1} L_i \cdot L_j \sim \delta_{ij} \; (= 0 \; for \; i \neq j) \tag{4}$$

Sensor occupancy is the quantitative measure of number of hits registered by the sensor. If sensor's occupancy is high enough along at least one of the coordinates, it yields that differing order contributions are independent.

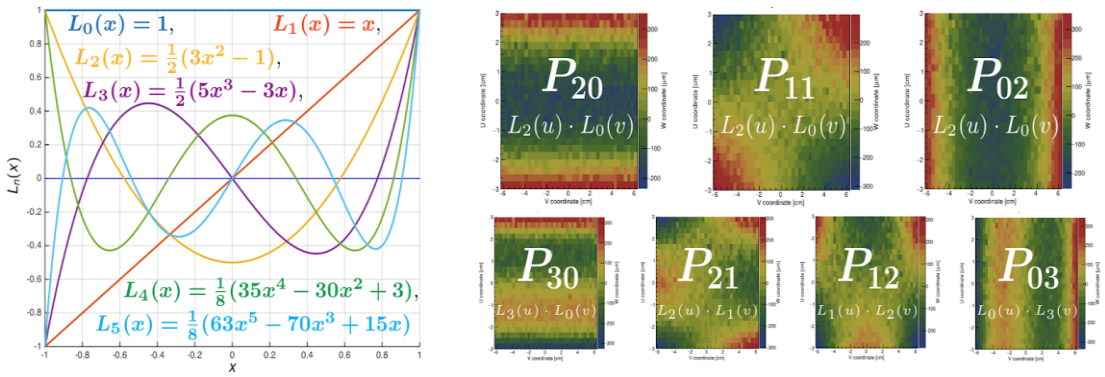

Figure 4.4: Legendre polynomials (left) and surface deformation parametrization (right) using the polynomials

4.4 Monitoring quality of comic tracks tracking in vertex detector

Cosmic tracks can serve as an effective tool for vertex detector alignment evaluation. Use of cosmic particle trajectories offers multiple tracking-benefitial possibilities, including fitting hits distributed throughout the entire volume of vertex detector (crossing both adjacent detector half shells) , using simple track-finding method, obtaining clear data without fake hits and the relatively easy elimination of incorrectly reconstructed hits.

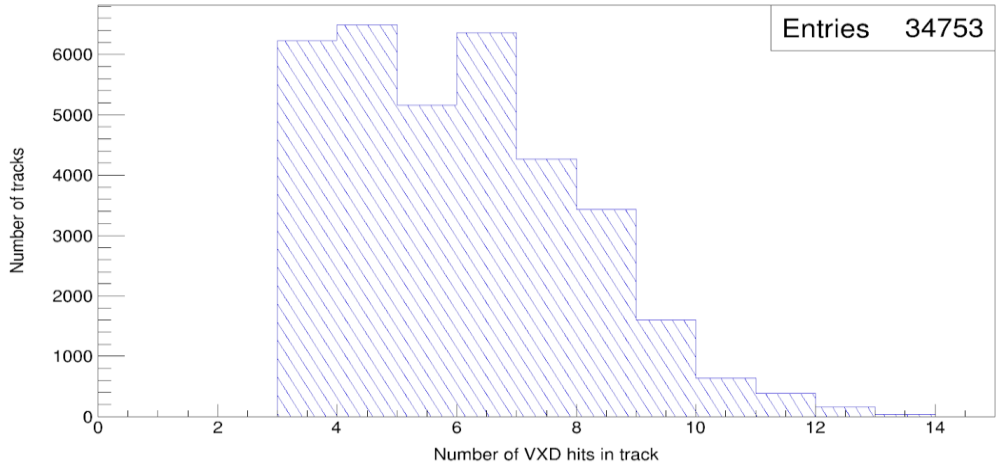

Figure 4.5: Number of hits associated with reconstructed cosmic track generated by MC analysis

Several other tracking-related quantities can be used for quality evaluation of cosmic tracks. The standard ones are number of reconstructed tracks, number of hits

associated with a cosmic track (Figure 4.5) or χ^2 /Degrees of freedom as χ^2 value of fitting result divided by number of degrees of freedom corresponding to a track (Figure 4.6).

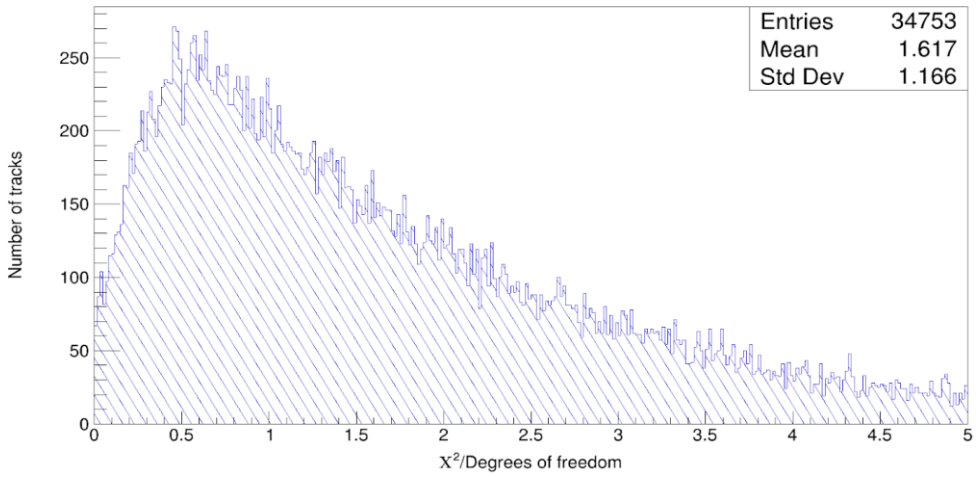

Figure 4.6: χ^2 distribution value divided by number of degrees freedom for MC simulation.

On the other hand, so-called"occupancy plots" reflecting number of associated hits with an incident sensor can be used for monitoring of track properties as functions of alignment or track reconstruction parameters. It is convenient to organize occupancy plots as a function of geometrical parameters of vertex detector as in Figure 4.7.

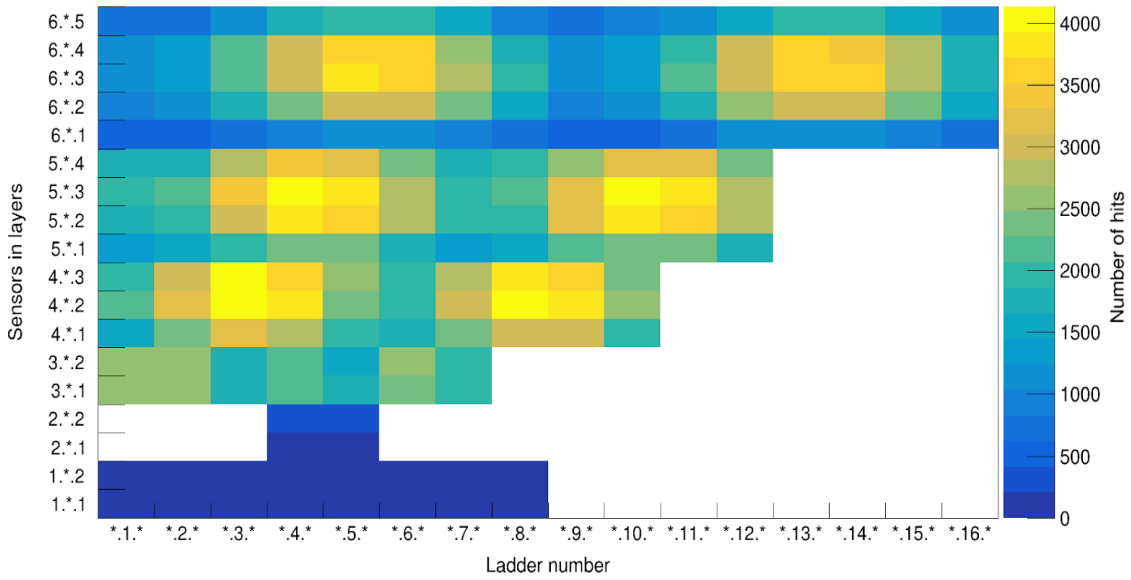

Figure 4.7: Number of associated hits with a sensor

Cosmic tracks which pass through the full vertex detector body are perfect candidates for monitoring and validation of vertex detector. One of the quantities worth keeping track of can be the number of hits per layer, dependent on layer number (Figure 4.8). This information helps to determine quality of alignment as it takes into account all sensors used during the reconstruction procedure. Cosmic tracks are able to connect some parts of vertex detector, which cannot be connected solely by using beam data (e.g. bottom and top half of the detector).

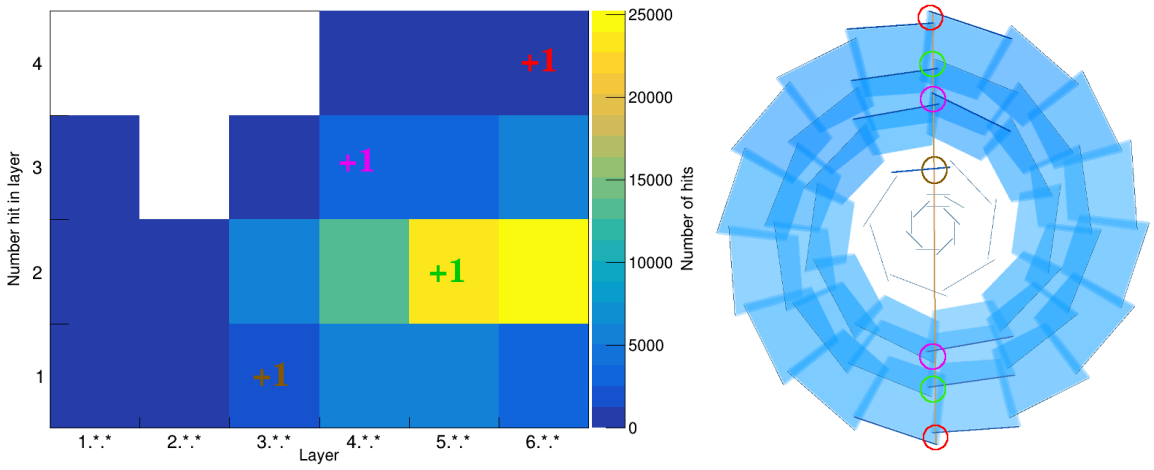

Figure 4.8: Monitoring plot and event display for MC simulation - Monitoring plot (left) shows result for MC simulation and event display corresponding to a single event (right) explains filling of 2D histogram bins. Red circles label four hits in sixth layer (right) and cell labelled "+1" indicates where processed information belongs. Other layer and associated hits are labelled different colors.

4.5 Validation of the vertex detector alignment

Monitoring of alignment parameters can be done in various ways. One of the useful methods is monitoring the quality of reconstructed data per each sensor. Different quantities are being taken into consideration in order to obtain realistic results and to increase the precision of alignment parameters.

For example, a very important information is presented by "hit map" plots which show the frequency of recorded hits in each part of sensor (Figure 4.9). This data can provide very important information about functionality of the readout system,

possible failures during reconstruction procedure and effects of trigger system on sensor occupancy.

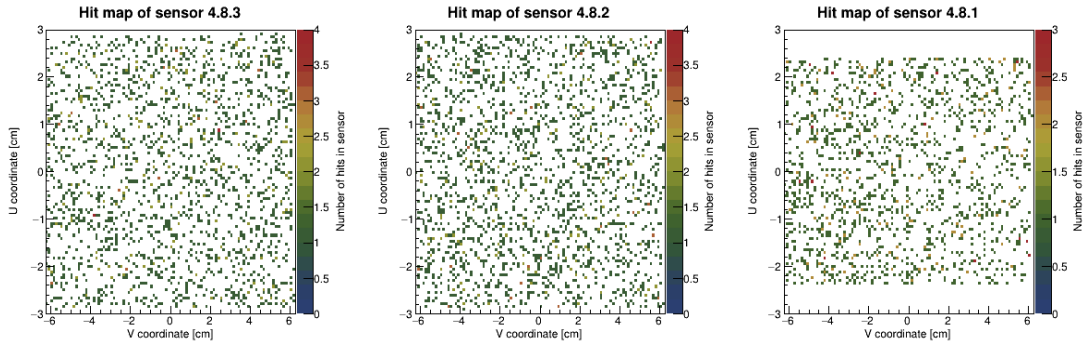

Figure 4.9: Hit maps of sensors in ladder 4.8 showing distribution of occupancy obtained using MC simulation. Right sensor is a slanted sensor and projected size is smaller in comparison with other rectangular sensors. This is caused by the dependence of strips pitch size on *u* and *v* coordinates.

.

Standard method used for validation and monitoring of alignment procedure uses hit to track based residual distribution (Figure 4.10). Residual distribution can be, without difficulties, determined for each sensor. That allows for a quick and easy way to check for deviations from correct position of sensors and quality of fitting. Residual distribution also help estimate needed corrections.

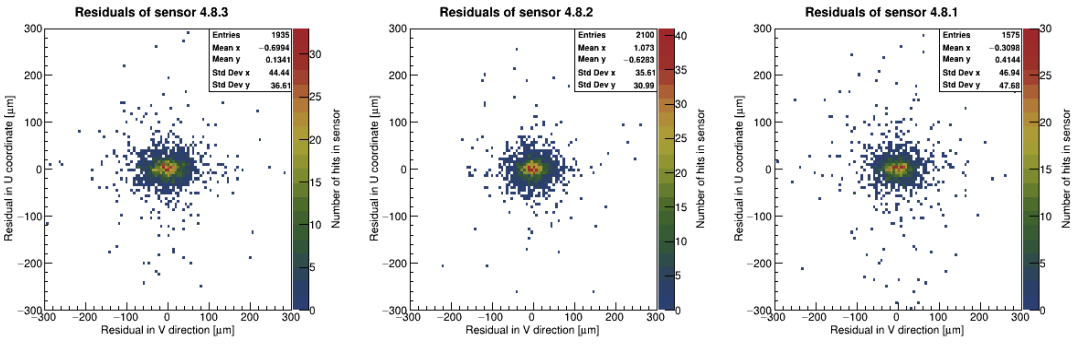

Figure 4.10: Hit to track based residual distribution of sensors in ladder 4.8 for MC simulation graphically illustrates precision of measurements.

The surface deformations can be monitored and validated using residuals corresponding to the *w* coordinate. However, measurement results are provided in *u*

and v local coordinates. The w coordinate should therefore be estimated from these results. For very small surface deformations following formulas can be used [8]:

$$r_W = r_U \, tan(\alpha_U) \quad (5)$$

$$r_W = r_V \, tan(\alpha_V) \quad (6)$$

where $r_{U,V,W}$ are corresponding residuals and tan $\alpha_{U,V}$ are slopes of track in a sensor. The illustrative algorithm for the w coordinate estimation using 2D measurement results is explained in steps in Figure 4.11.

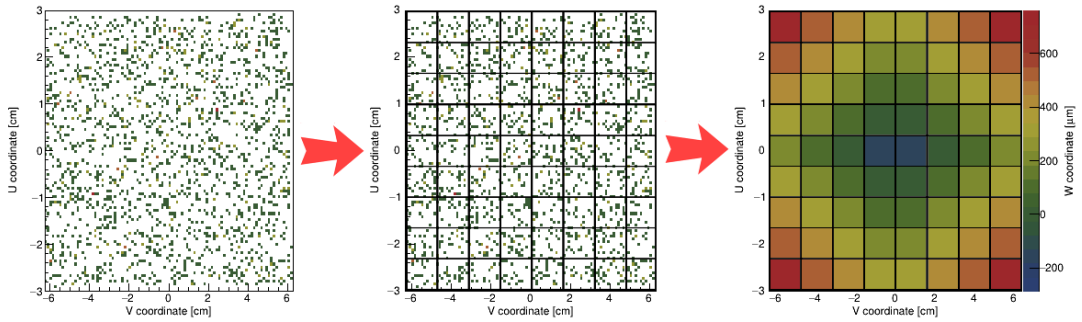

Figure 4.11: Estimation of the w coordinate – Algorithm explanation in 3 steps - 2D position measurement on surface of a sensor (left picture) is the starting point. Subsequently, sensor's surface is divided into m × n matrix (center). Average value of the w residual is then estimated for each cell of the matrix with the use of formulas (5) and (6) for all hits in cell. Each contribution to average value is weighted by squared slopes of track in sensor (right). The estimation should be done for both measurements.

5 Cosmic Rays

Relativistic ionized nuclei hit the Earth's atmosphere with a rate or approximately 1000 s^{-1} m^{-2}. Their energy spans from hard to detect tens of MeV usually up to several hundreds TeV [14][16]. Based on their origin, primary and secondary components of cosmic radiation are distinguished.

The atmosphere is an unavoidable very effective calorimeter for a passing charged particle. Most of the air showers created in the top upper layers of the earth's atmosphere have hadronic origin thanks to the abundance of primary protons. The character of the shower is not only dependent on the original energy of the incident particle but also on the creation altitude [15][17].

Hadronic, leptonic and electromagnetic showers and subshowers, components of a cosmic air cascade, are generated by a process starting with initial interaction resulting in production of pions (neutral, positive and negative) and kaons (positive and negative), mesons of a very short lifetime (of order or nanoseconds) almost immediately decaying into muons and, in case of a neutral pion, and a photon pair [18]. Following interactions include ionization, bremsstrahlung, multiple scattering, Compton and Rayleigh scattering for charged particles accompanied by photons interacting via photoelectric effect and pair production followed by annihilation processes [14].

Muons, which make up the leptonic component of cosmic air cascade, are the most abundant particle reaching the Earth's surface. Muons are created in a decay channel of charged mesons at the altitude of approximately 15 km. The average energy loss of a muon thanks to ionization when passing through the atmosphere reaches up to 2 GeV.

If the energy of the penetrating particle is high enough for the created shower to be detected at the earth's surface, it brings along a great amount and variety of information. When reaching the ground level, muons, as highly energetic and relatively little interacting particles, can serve as a very useful tool for detector calibration. They are successfully used for timing synchronization, tracking and energy calibration. Thanks to low amount of energy they deposit in materials muons are able to pass through the entire volume of the detecting device. Their reconstructed trajectories are, in presence of no magnetic field, almost perfectly linear, which allows

for their use as a valuable tracking and alignment tool [19]. For the purpose of alignment procedure muon tracks help software analyzing tools connect signals measured by two separate opposing parts of the detector. For these reasons muon tracks were used for the alignment procedure in this work.

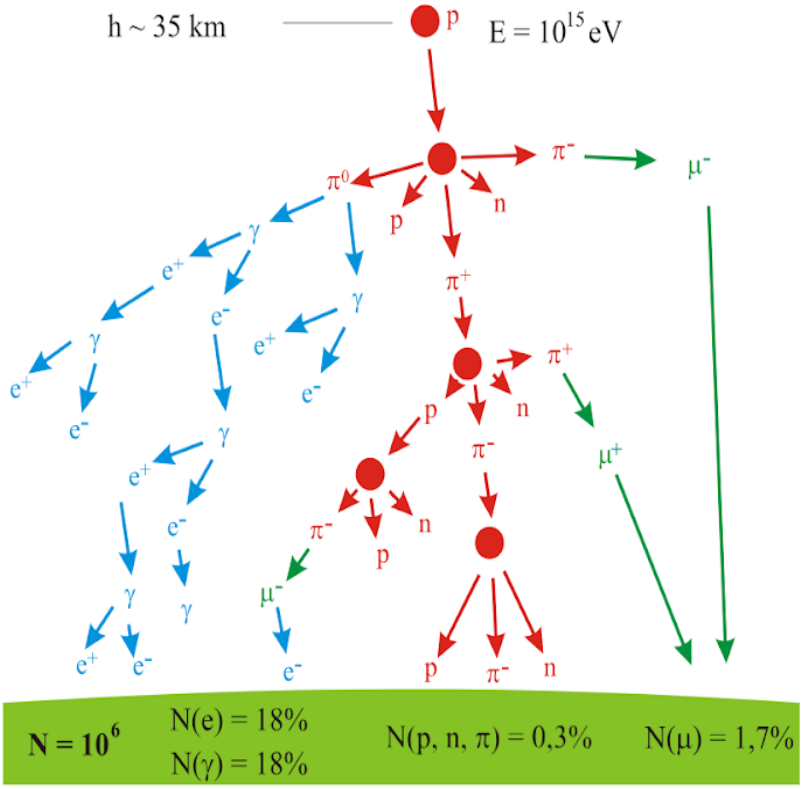

Figure 5.1: A scheme of cosmic ray shower picturing hadronic particle interactions dominated cascade core [20]. In figure we can see electromagnetic (blue), hadronic (red) and leptonic (green) part.

6 Results of validation and monitoring

Different possible ways of validation and quality monitoring of the alignment procedure were discussed and illustrated in Chapter 4 using MC simulation.

Author's input to results presented in this chapter focused on analysis of obtained datasets in order to evaluate alignment procedure impact on quality of reconstructed tracks. These datasets contained results of individual alignment iterations applied to the collected data. Cosmic tracks were used as a validation tool offering the very first possibility to apply track based alignment method to the Belle II vertex detector.

Results of the alignment procedure were analyzed using *ROOT* macros, written by the author for this purpose, in order to compare statistical properties of collected data and interprete them in an illustrative way by generating comparative plots.

The quality monitoring analysis consisted of two separate parts. In the first part, all detecting sensors were treated as rigid body objects. The track based alignment procedure, applied in this section, determined rigid body parameters, which describe shifts and rotations of sensors.

Results and quality assessment are represented in the following chapter, where the author discussed individual aspects and purpose of each covered property. Observed patterns and characterics dependent on number of alignment iterations and alignment procedure quality were given special attention.

The second part of the alignment studies is motivated by the possibility to improve alignment quality by detecting surface deformations. Fitting procedure applied by the author to the *w*-projection of measured quantities elaborated on thesis consultant’s idea to find a way to get a grasp of planar deformations’ impact on alignment quality. *W*-residual distributions are used in the studies and fitted parameters values are applied in addition to rigid body alignment procedure corrections.

6.1 Alignment quality monitoring

In the first part, results of four separate alignment iterations are compared and studied. Higher quality cosmic rays data sets of reconstructed tracks were selected for

the alignment validation in order to achieve higher precision. From all the collected cosmic data the choice was narrowed down to run numbers 173, 174, 175, 189 and 190 [8]. The selection was made under imposition of several limiting constraints, e.g. restrictive χ^2 threshold selecting tracks with converging nature, minimizing the function value.

The alignment parameters determination focused on detection of shifts and rotations of individual sensors. Parameter values associated with 6 rigid body degrees of freedom were determined by the alignment procedure. Planar deformations, which are to be discussed in the latter section, were not taken into consideration. Conditions of fixed positions of the vertex detector half-shells and ladders were used, as well as certain hierarchical constraints were imposed on sensors and ladders in the fourth, fifth and sixth layer. After each of four repeated iterations, corrections to iteratively updated positions were applied.

6.1.1 Residual distributions

The residual distribution corresponding to both, the *u* and the *v* direction of local coordinate system indicate significant improvement achieved by application of alignment corrections. In the following Figures 6.1 and 6.2, residual distribution describing precision of position measurement before the alignment is depicted in black, while the final stage, after four alignment iterations and applied corrections to initial position, is drawn in red color. These figures illustrate statistical results for all analysed tracks. The residual distribution, with each iteration, becomes more centered around zero value and its standard deviation observably decreases in size. These trends indicate higher hit to track correspondence and decreasing deviations from real particle trajectories. After the fourth alignment procedure iteration, the value of standard deviation decreased by three quarters in size in comparison with the nonaligned detector distribution.

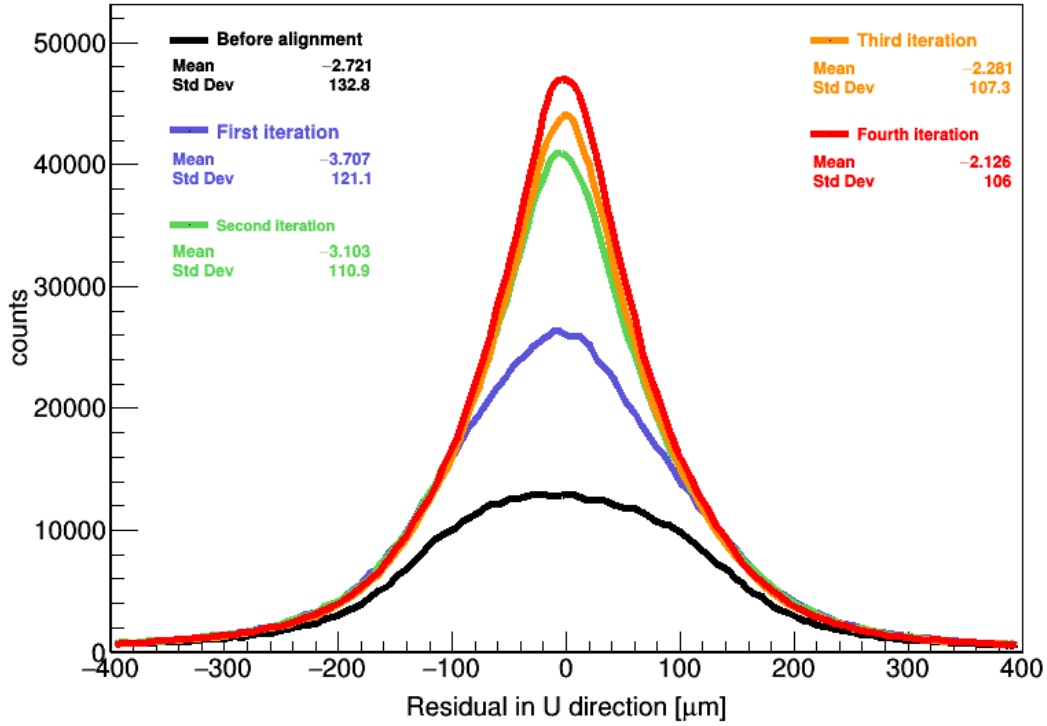

Figure 6.1: Residual distributions in the *u* direction for all sensors

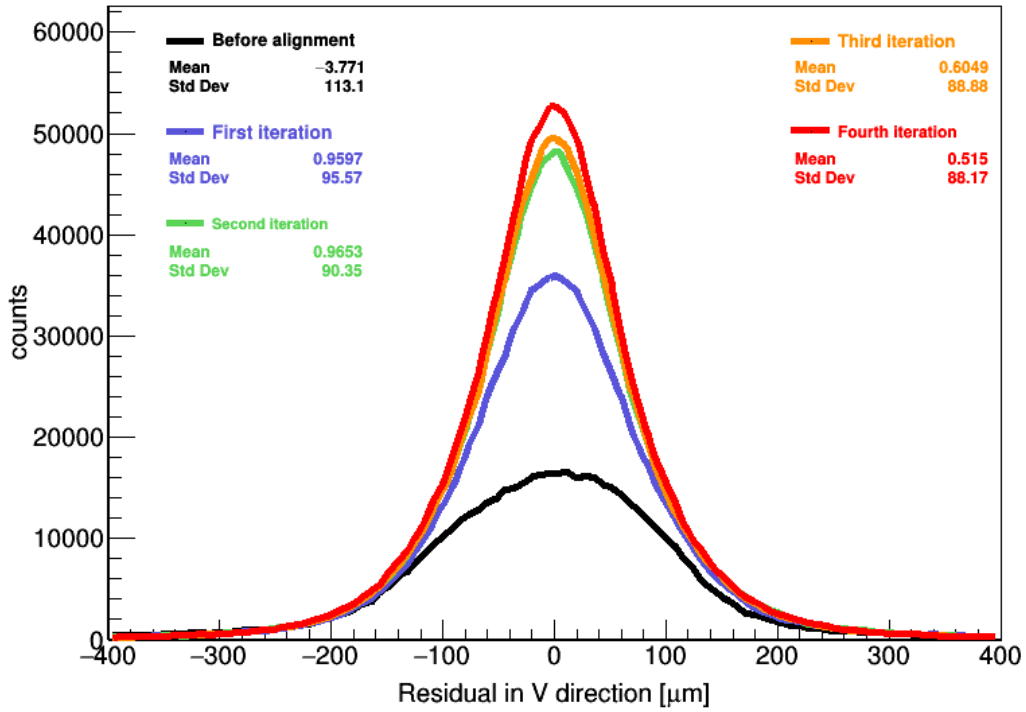

Figure 6.2: Residual distributions in the *v* direction for all sensors

6.1.2 Number of hits per track

Another basic characteristic of a reconstructed track is a number of its associated hits. The better the precision of hit detection and localization is, the greater is the number of hits corresponding to a fitted particle trajectory. This is caused by minimized discrepancies between the measured and actual hit position. Reconstructed tracks with high precision are more likely to consist of more particle generated hits. Figure 6.3 therefore helps with tracking quality monitoring.

As can be seen in this figure, for the histogram outlined in black, corresponding to nonaligned geometry, most of the reconstructed tracks consis only of 4-5 associated reconstructed hits. For the final fourth alignment iteration, marked red, the number of hits per track has increased significantly. When compared with Figure 4.5 showing expected shape of number of hits depencency on iteration number, the final aligned geometry resembles very similar characteristics as MC simulation.

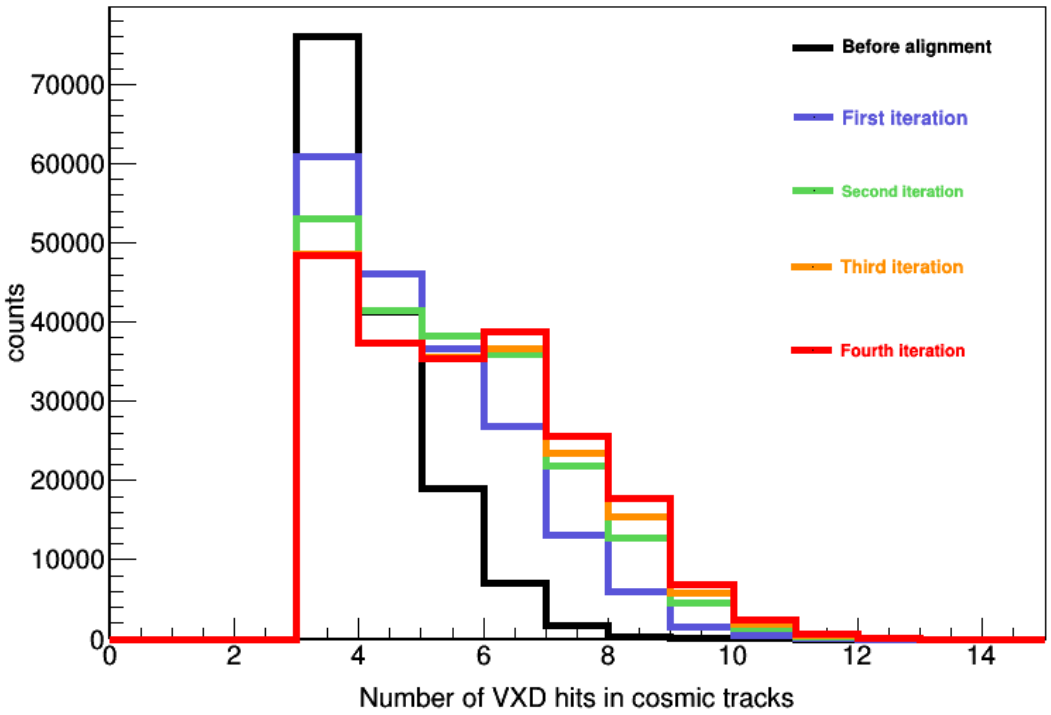

Figure 6.3: Distributions for number of VXD hits in cosmic tracks

6.1.3 χ^2/Number of degrees of freedom

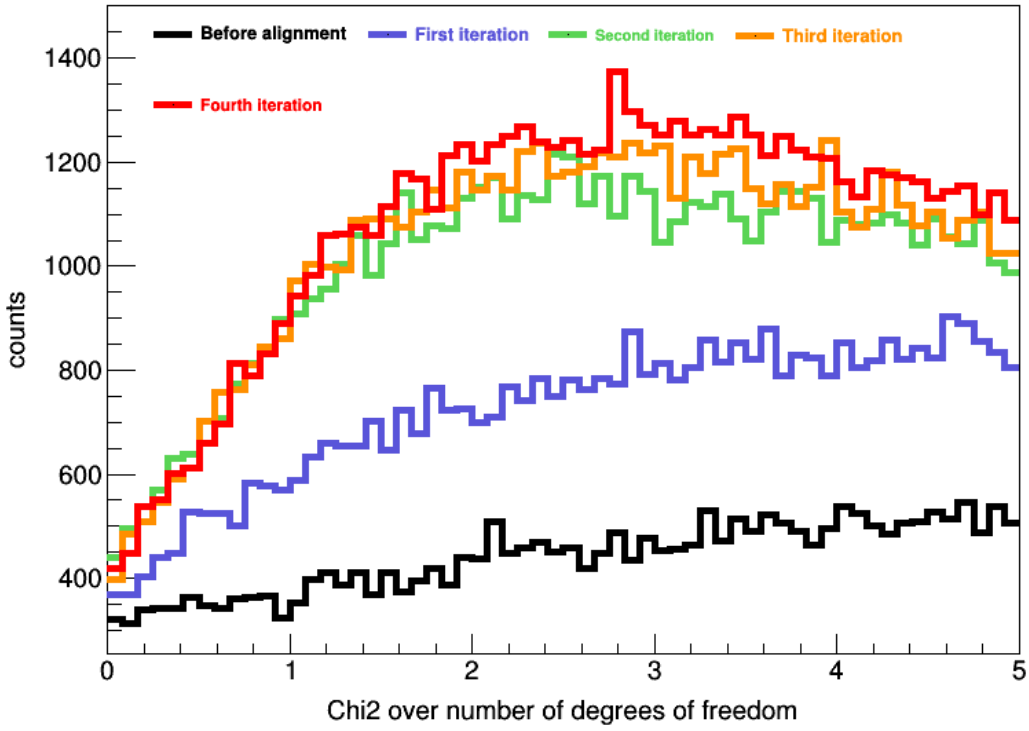

Figure 6.4: χ^2 over degrees of freedom distributions for analyzed iterations

The χ^2 over number of degrees freedom distributions (Figure 6.4) represent quality of fitting collected VXD hits. Improvements are most obvious for the first three alignment iterations. The quality of reconstructed fitted trajectories increased significantly as the precision of hit reconstruction improved with more accurate relative positions of detecting sensors. These relative geometry changes are functions of alignment-based corrections.

Fluctuations observable for the latter iterations can be a result of applying solely linear fits to collected cosmic data. Fitted parameters did not change dramatically within the 2 last sets of iterations. This implies converging nature of spatial positioning of detector components. However, as mentioned before, the convergence of χ^2 function itself does not suffice as a proof of succcesful alignment of detector geometry as the function could have possibly not reached its global minimum. That might lead to biased set of alignment parameters. Local minima of the function put another obstacle into the way to a perfectly aligned detector (and therefore also precise data analysis and reconstruction). These are, however, not a subject for a discussion in this thesis.

With the increasing number of repeated iterations, shape of the resulting functional curve approaches theoretically expected dependency trend predicted by the χ^2 over number of degrees freedom distribution corresponding to MC simulated data pictured in Figure 4.6.

6.1.4 Sensor occupancy

Two dimensional histograms in Figure 6.5 and 6.6 show comparison of sensor occupancy for a nonaligned detector and a geometry after the fourth iteration of alignment procedure. As can be seen, the occupancy did, in general, increase. However, a distinct pattern is noticeable especially in the layers with the highest occupancy (the fourth and the fifth layer). The increasing number of hits per sensor speaks of improving sensor position determination. Precise relative positions of detecting sensors mean better accuracy in hit reconstruction. This leads to higher quality tracking and larger number of track associated hits. Reconstructed tracks are therefore more reliable and valuable for monitoring and validation procedures.

Figures 6.5 and 6.6 provide illustration of positive effect of alignment procedure on number of detected hits per sensor. Alignment determined corections to sensor positions not only helped increase the occupancy of sensors in every layer, but also magnified the effect of geometry on rate of hit detection experienced by differently oriented and situated detector sensors.

Since cosmic ray data sets, which were subject to this analysis, were no longer generated by a simulator in a homogenous manner, even distribution of registered hits for all sensors wasn't expected.

Cosmic tracks used for these studies are created by cosmic particles, mostly muons, with very low impact parameters. As previously stated, their paths are, thanks to this fact, detected in both opposing half-shells of the detector. Cosmic particles pass through the entire detector body in more or less vertical direction. This natural tendency leads to distinguishable patterns on occupancy plots of detector sensors. *X*-projections of the 12th row of 2D histogram (Figure 6.7), where the pattern seemed to be most distinct according to Figure 6.6, illustrate this behavior.

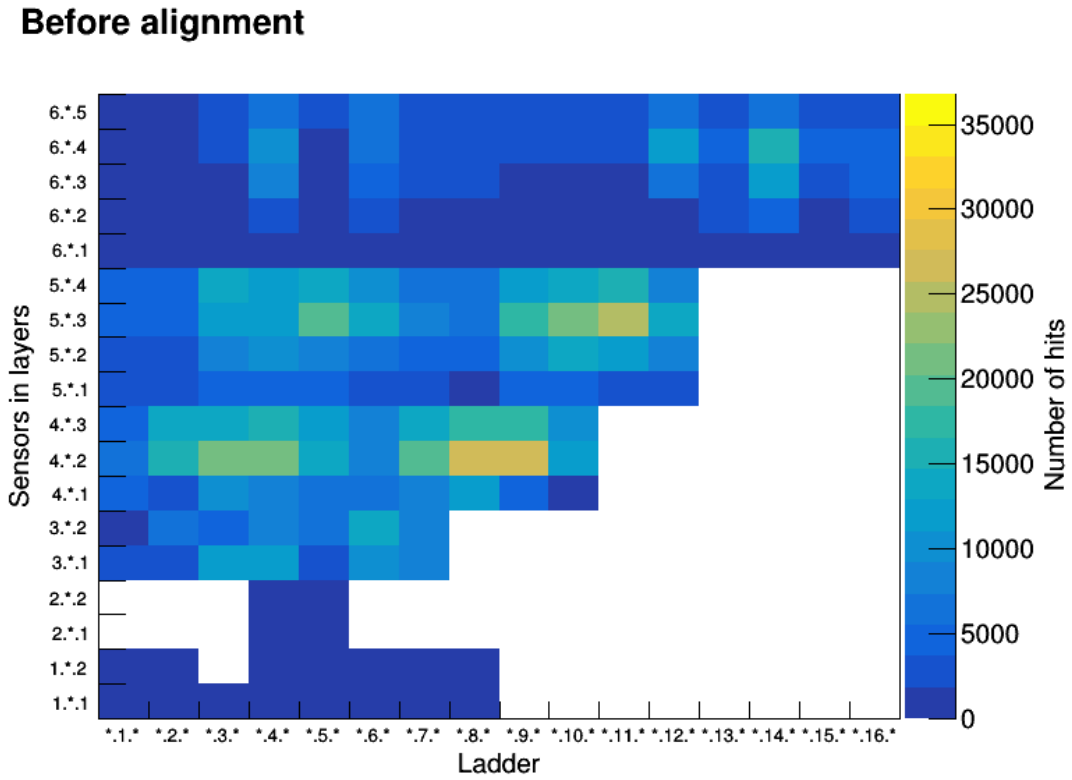

Figure 6.5: Occupancy of individual sensors for non-aligned detector

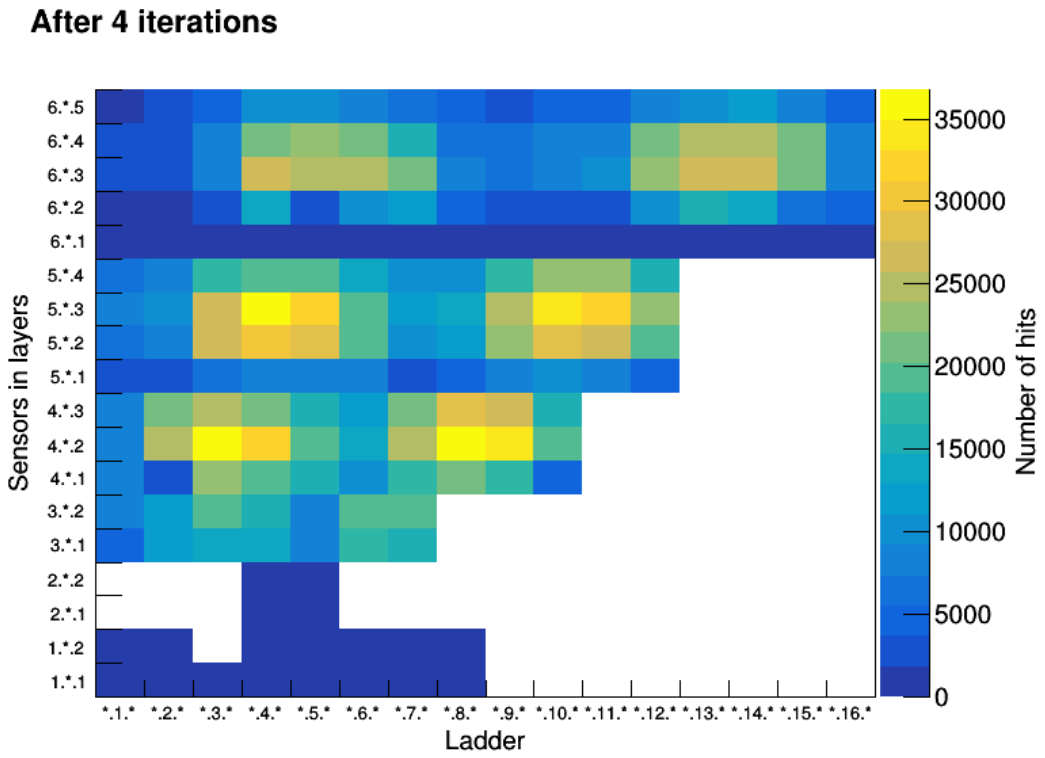

Figure 6.6: Occupancy of individual sensors after the last iteration

Bin contents of the compared histograms represent occupancy of 5.*.3 sensor at given angular position after each alignment iteration. Lower occupancy of slanted

sensors can be observed as well as significantly lower number of hits detected in parts of the detector with their active area in a shallow incident angle to passing particles. When working with cosmic data, number of registered hits is significantly dependent on the geometry of the detector.

This dependency can be understood better when looking at the geometrical spatial placing of sensors, based on the geometry scheme of the detector pictured in Figure 2.3 and 2.5.

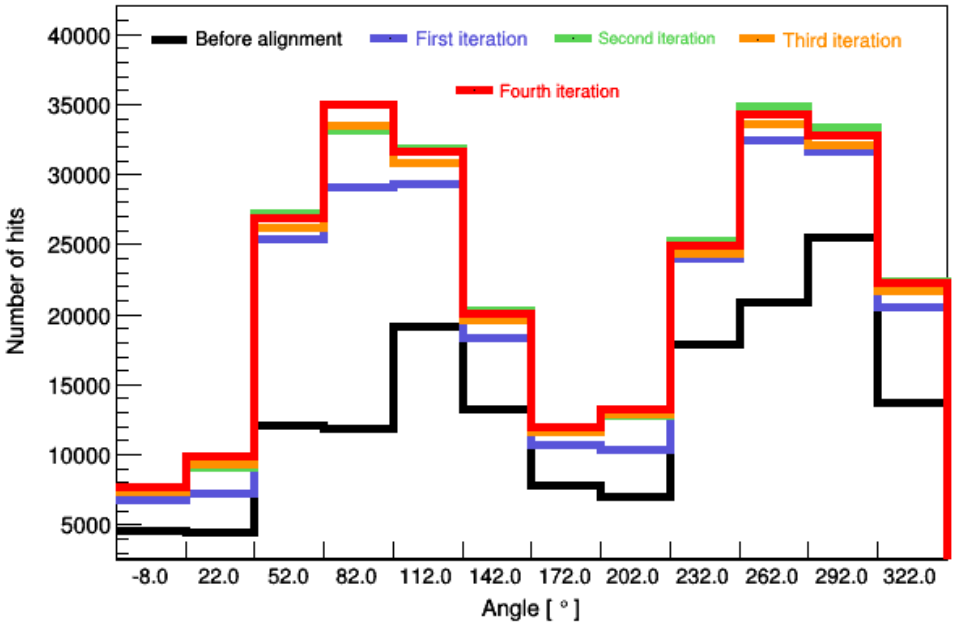

Figure 6.7: Occupancy of 5.*.3 sensor for different iterations

6.1.5 Number of hits per layer

Figure 6.8 on the following page presents number of hits per layer as a function of alignment iteration. As can be seen, each iteration produces different results of this sensitive technique used for alignment procedure validation. As the top left figure indicates, the alignment procedure starts out with randomly, generally imperfectly, organized hits in track dependent on number of hits in layer. Each next iteration approaches the expected behavioral pattern pictured in Figure 4.8 a little more. The first iteration showed noticeable improvement in number of recognized hits for the fifth layer, while the following iterations led to increasingly higher and higher

occupancies of the third, fourth and the sixth layer. The fourth iteration is very similar to the expected distribution pattern according to Monte Carlo studies (Figure 4.8).

The most occupied row in the 2D histogram corresponds to 2 hits per track detected in a layer. This behavior meets the expectations, since a higher number of hits per layer indicates occurance of a so called “overlap”, when the particle trajectory manages to traverse the detector via spots were two sensors in the same layer overlap. Smaller number of hits per layer corresponds to a trajectory passing through the detector volume in a direction signifcantly deviating from orthogonal orientation to the detecting sensor.

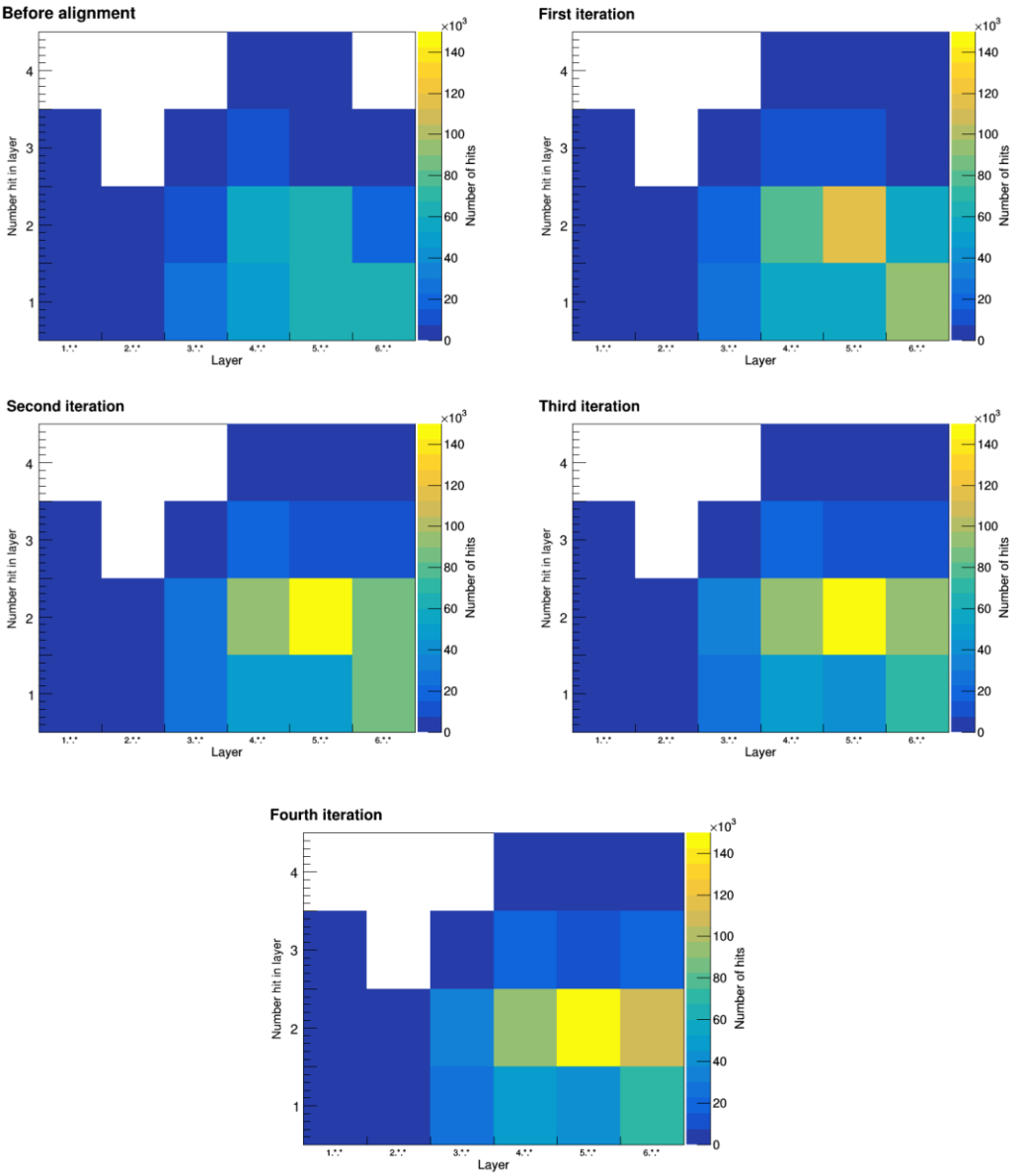

Figure 6.8: Number of hits per layer for each iteration.

6.1.6 Rate of reconstructed cosmic tracks

Figure 6.9 represents the dependence of rate of reconstructed cosmic tracks in vertex detector on the number of alignment iterations. It can be seen that the cosmic rate increases as a function of iteration. It shows the positive effect of alignment corrections applied in each iteration. Improvement in position accuracy and hit reconstruction precision lead to higher precision of tracking procedure. Number of reconstructed trajectories as a function of iteration can be, up to a satisfactory level, represented by a function:

$$f(x) = \frac{Ax}{(B+x)} \tag{7}$$

Fitting the data with this function results in free parameters values A = 4.69 ± 0.01 and B = (6.39 ± 0.07)·10^{-1}.

For greater number of procedure iterations the rate of reconstructed cosmic tracks of approximately ~5 s^{-1} is expected. As can be seen, based on previously listed characteristics and observed behavorial patterns in tracking dependent statistic quantities, the quality of reconstructed tracks can be reliably estimated. The success of alignment method in quality monitoring and evaluation can also be illustrated by Figure 6.9. As can be seen, the fourth alignment iteration approaches asymptotic value satisfying well, which leads to a conclusion, that not many more iterations woud be needed in order to achieve very high level of alignment precision.

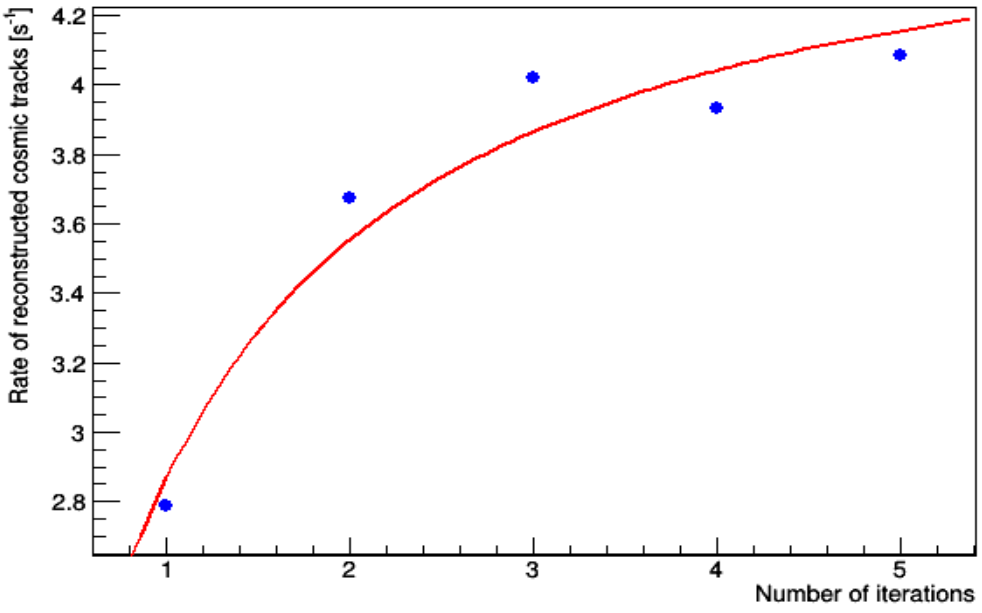

Figure 6.9: Rate of reconstructed cosmic tracks as a function of number of iterations

6.2 Estimation of alignment parameters from validation

The effects of misplacement and general misalignment of detector geometry on monitoring tools, which were developed for this purpose, were discussed in the previous section. This monitoring method proved to be successful when determining rigid body parameters of sensors and their corrections. The precision of track reconstruction procedure increased significantly, however, not up to a satisfactory level.

Extending alignment procedure to surface deformation parameters leads to even better precision of measurements. The main goal of the second part is to analyze and visualize validation and quality monitoring results and reliably detect and interpret surface deformations of sensors.

Based on working with MC simulated datasets and basic track characteristics it was observed, that the alignment parameters can be estimated from validation procedure using residuals plots (Figure 6.10). Shifts in the *u* and *v* direction can be directly estimated from mean values of corresponding residual distributions without use of Millepede II algorithm.

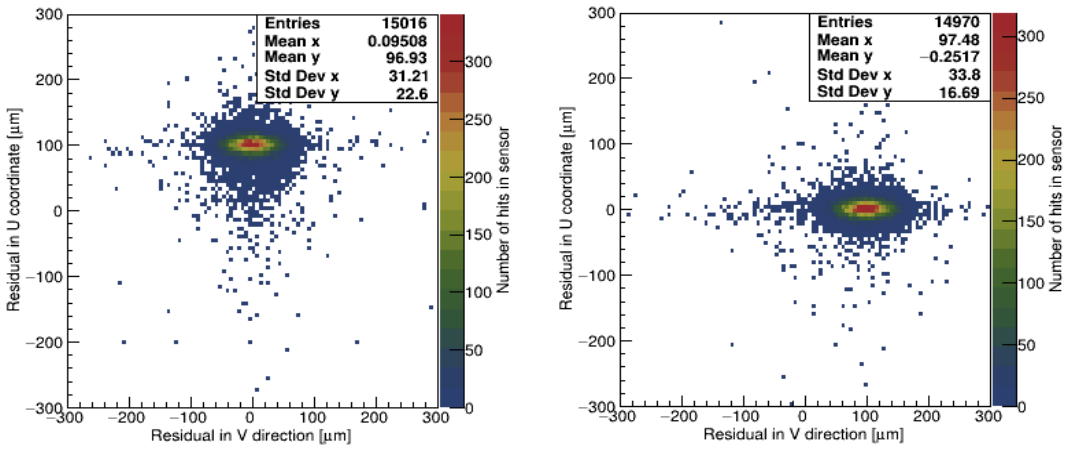

Figure 6.10: Estimation of shifts in the *u* (left) / *v* (right) direction by about 100 µm using residuals distribution obtained from MC simulation

Attempt to fit validation plots proved to be successful in determining several other alignment parameters. The fitting part of the procedure is done in two steps. Firstly, the measurement results undergo transformation from a sensor's local

coordinate system to Legendre system. Subsequently, the obtained data are fitted by 2D Legendre polynomial function:

$$\begin{aligned} w(u,v) \; = P_W \cdot \; L_0(u) \cdot L_0(v) \; + P_\alpha \cdot L_0(u) \cdot L_1(v) \; + P_\beta \cdot L_1(u) \cdot L_0(v) + \\ + P_{20} \cdot L_2(u) \cdot L_0(v) + P_{11} \cdot L_1(u) \cdot L_1(v) + P_{02} \cdot L_0(u) \cdot L_2(v) \; + \\ + P_{30} \cdot L_3(u) \cdot L_0(v) + P_{21} \cdot L_2(u) \cdot L_1(v) + \; P_{12} \cdot L_1(u) \cdot L_2(v) \; + \\ + P_{03} \cdot L_0(u) \cdot L_3(v) \; , \end{aligned} \tag{8}$$

where L_N represents Legendre polynomials (from Figure 4.4) , P_M stands for alignment corrections desired to be determined. These process results in a set of fitting parameters. Each these values is associated with a different surface deformation (see Figure 4.4).

Illustration of fitting procedure is descriptively explained by Figure 6.11.

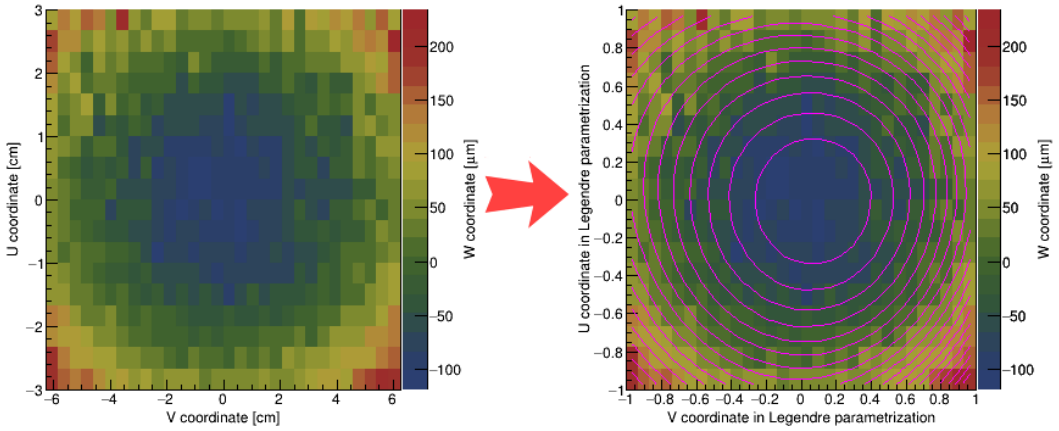

Figure 6.11: Fitting algorithm of surface validation plot for determination of additional alignment parameters: Figure shows combination of P_{20} and P_{02} parameters corresponding to deformation of about 100 µm and their visulisation by MC simulation.

Once having applied the fitting procedure on MC generated data, several alignment parameters were successfully determined using residual and surface validation plots. Both already mentioned methods (rigid body paramateres determination by the software monitoring tools and their estimation from validation plots) present a possibility to estimate 3 shift parameters (P_U, P_V, P_W) and two rotation

parameters (P_α, P_β). The fitting procedure allows for determination of at least three additional surface deformation parameters (P_{20}, P_{11}, P_{02}, P_{30}, P_{21}, P_{12}, P_{03}). One of the biggest disadvantages of the method using validation plots is the inability to estimate P_γ parameter associated with angle γ.

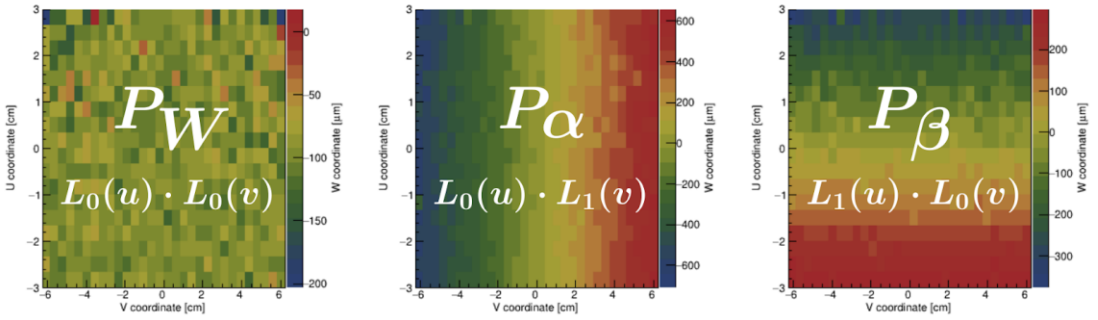

Figure 6.12: Illustration of initial misalignment of alignment parameters P_W (left), P_α (center) and P_β (right): Figure shows validation of misalignment about 100 μm for P_W and 0.1 rad for P_α, P_β

Illustration of particular results of the validation and fitting procedures, tested on MC analysis using generated non-aligned data values, is presented in Figure 6.12.

In the second part, all the collected data were used for the analysis. No quality restrictions were imposed which resulted in higher deviations and poorer quality of reconstructed hits. On the other hand, greater number of recorded and reconstructed tracks allowed for better and more reliable statistics carrying more information about sensor characteristics.

In the first part of the applied analysis, the presented model suggested that the hit rate keeps increasing proportionaly to the number of alignment procedure iterations until it reaches the expected value. However, the detected rate of events analysed in the latter section is higher because of the much lower quality threshold imposed on the data entering the analysis pocedure.

Approximation of alignment parameters based on the validation procedure was tested on three received sample datasets – Before alignment, containing initial sensor misalignmnet data, Rigid body, which corresponds to a dataset to which corrections of shift and rotation alignment parameters were already applied, and After alignment, with shift, rotation and surface corrections applied.

6.2.1 Sensor 4.3.2

Results obtained after each of two separate steps of the procedure described above applied to sensor 4.3.2 are best demonstrated by changes in corresponding validation plots, showed in Figures 6.13, 6.14, 6.15.

As can be seen from the values of alignment parameters listed in Table 4.1, the sensor initially exhibited detectable shift in the *u* direction, rotation around the *v* axis as well as several planar deformations. Values of parameters corresponding to listed sensor misplacements are larger than the calculated monitoring tool error. The error of monitoring tool was estimated by fitting the validation plots by the first constant term from Equation (8).

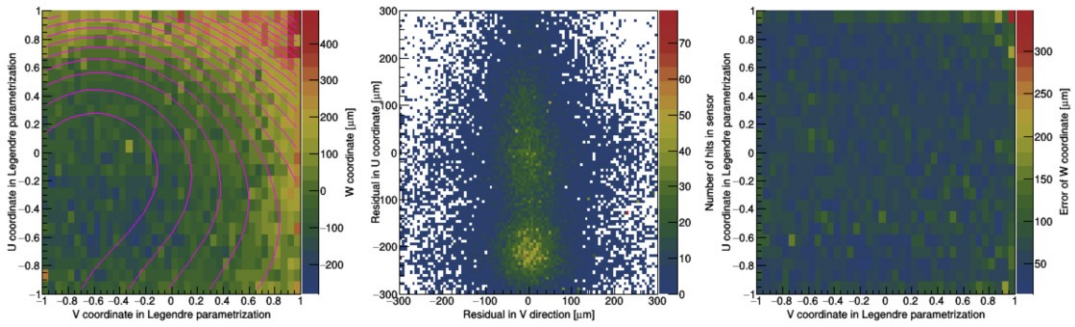

Figure 6.13: Initial misalignment of sensor 4.3.2 represented by validation plots and residual distribution - surface validation plot fitted by the *w(u,v)* function (on the left), corresponding residual for the *u* and *v* directions (center) and a two dimensional representation of bin errors of the planarity validation plot.

After the first step of validation procedure, once the corrections to estimated shift and rotation parameters were applied, a noticeable difference could be observed in obtained validation plots shown in Figure 6.14.

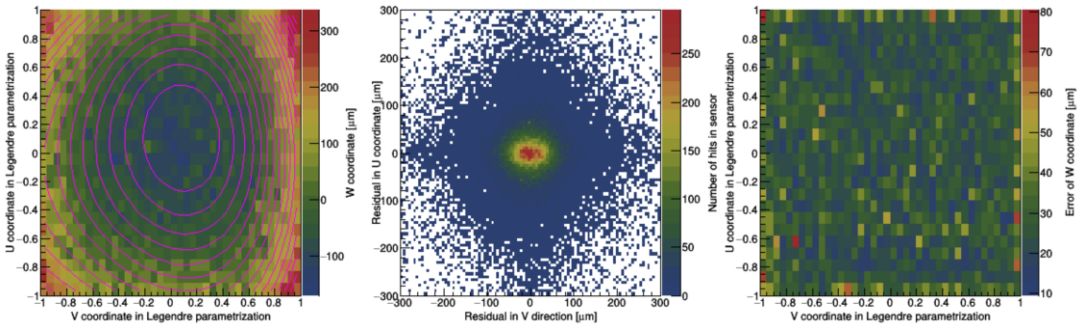

Figure 6.14: Planarity validation plots of sensor 4.3.2 under shift and rotation corrections

From Figure 6.14 it can be seen that the effect of corrections of estimated parameters is relevant but not satisfactory. The first of the validation plots in Figure 6.14 no longer shows signs of misalignment connected to rigid body paramaters (as can also be understood from the second parameter column in Table 6.1). Unlike rigid body parameters, effects of planar deformations are still observable in validation plots. Impact of these deformations was eliminated by the fitting procedure.

Figure 6.15 presents validation results after shift, rotation and surface corrections are applied. Comparison of Figures 6.14 and 6.15 suggests substantial improvements in sensor misalignment minimization. As expected, surface validation plot shows no more signs of surface deformation of sensors after having applied all calculated correction determined from parameter values. Numerical results can be found in Table 6.1.

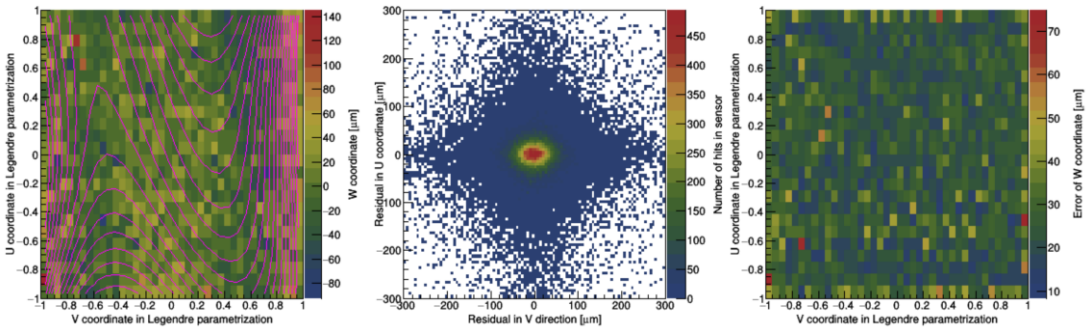

Figure 6.15: Final validation plots of sensor 4.3.2 obtained as a result of fitting procedure

Parameter $[\mu m]$	*Before alignment*	*Rigid body*	*After alignment*
P_U	-64.87 ± 0.69	-0.99 ± 0.27	-0.88 ± 0.22
P_V	2.5 ± 0.40	-0.27 ± 0.27	-0.05 ± 0.23
P_W	3.93 ± 0.14	3.93 ± 0.14	0.17 ± 0.08
P_α	6.66 ± 0.39	6.66 ± 0.39	0.37 ± 0.14
P_β	64.76 ± 0.41	-0.96 ± 0.30	-0.95 ± 0.13
P_{02}	27.13 ± 0.47	97.31 ± 0.53	0.82 ± 0.17
P_{11}	25.60 ± 0.77	1.75 ± 0.48	0.21 ± 0.25
P_{20}	63.63 ± 0.49	65.01 ± 0.41	0.29 ± 0.16
P_{03}	-4.93 ± 0.57	24.33 ± 0.60	2.19 ± 0.19
P_{12}	29.03 ± 0.93	26.26 ± 0.94	1.24 ± 0.30
P_{21}	9.83 ± 0.91	2.50 ± 0.78	-0.49 ± 0.28
P_{30}	16.53 ± 0.55	6.51 ± 0.45	-0.21 ± 0.19
Monitoring tool error	57.61	24.42	23.12

Table 6.1: Values of estimated alignment parameters before applying corrections (2nd column), with corrections of shift and rotation misplacements (3rd column) and after surface deformation corrections (last column).

Success of the procedure is clearly exhibited by the vanishing values of deformation fitting parameters associated with individual steps of the monitoring process (Table 6.1). Values in the last column in Table 6.1 confirm conclusions suggested by graphical visualization of validation plots. Combination of rigid body paramaters and fitting parameters associated with surface deformations successfully eliminated impact of detector misalignment.

6.2.2 Sensor 3.3.2

Planarity validation plots obtained for sensor 3.3.2 (Figure 6.16) illustrate effects of sensor shift in the *w* direction and detectable rotation around the *v* coordinate axis. Numerical values of obtained fitting parameters listed in Table 6.2 complement the graphical interpretation.

The value of *w*-shift associated parameter is more than three times higher than the calculated monitoring tool error. This suggests that the shift plays a significant role in alignment and track reconstruction procedures.

Value of parameter corresponding to rotation by β angle, P_β, was calculated to be slightly bigger than the measurement uncertainty. Together with the parameter P_α, with its absolute value slightly below the monitoring tool error limit, these

deformations are expected to have non-negligible influence on the tracking precision. Therefore they are to be eliminated by the alignment procedure.

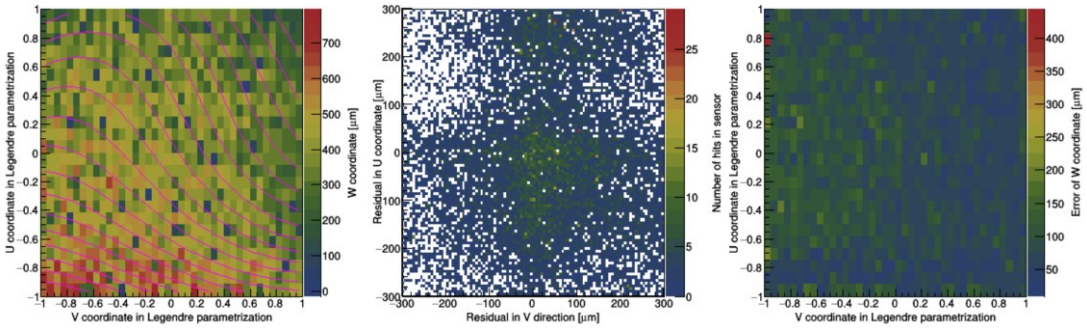

Figure 6.16 : Validation plots of sensor 3.3.2

Parameter	$[\mu m]$	*Parameter*	$[\mu m]$
P_U	-1.41 ± 1.1	P_V	32.39 ± 0.95
P_W	315.27 ± 0.57	P_{20}	27.27 ± 1.30
P_α	-67.87 ± 0.99	P_{03}	7.42 ± 1.50
P_β	-91.74 ± 1.01	P_{12}	-15.68 ± 2.23
P_{02}	-10.80 ± 1.29	P_{21}	10.04 ± 2.20
P_{11}	5.86 ± 1.73	P_{30}	-14.66 ± 1.48
Monitoring tool error			70.81

Table 6.2 : Values of alignment parameters obtained by the validation procedure

6.2.3 Sensor 5.10.3

Sensor shifts in direction of coordinate axes can be detected solely by analyzing the mean values of validation plot residuals. This approach is illustrated by Figure 6.17. Corresponding parameter values, determined from statistical characteristics of measured residual distributions, directly indicate the magnitude as well as direction of such a shift.

Besides the shift indicating parameter P_V, parameters P_W and P_{20} are also interesting in terms of alignment procedure. Their values, as can be seen in Table 6.3, reach or even exceed the monitoring tool error magnitude and therefore, in order to improve the detection precision and accuracy, need to be eliminated by the alignment procedure.

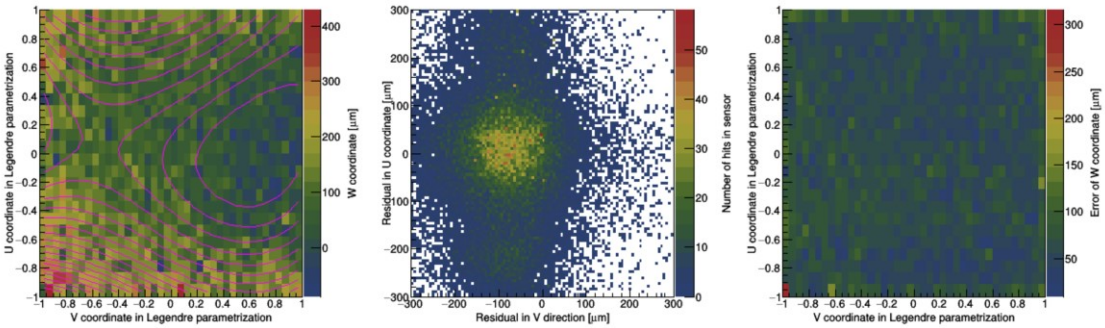

Figure 6.17: Validation plots of sensor 5.10.3 demonstrating shift in the *v* direction and planar deformations of the sensor

Parameter	$[\mu m]$	*Parameter*	$[\mu m]$
P_U	-1.28 ± 0.60	P_V	-76.86 ± 0.43
P_W	53.04 ± 0.24	P_{20}	82.33 ± 0.61
P_α	-39.69 ± 0.43	P_{03}	17.77 ± 0.50
P_β	-22.34 ± 0.54	P_{12}	-41.33 ± 0.92
P_{02}	-3.78 ± 0.41	P_{21}	-29.27 ± 1.03
P_{11}	23.39 ± 0.88	P_{30}	-9.17 ± 0.66
Monitoring tool error			55.27

Table 6.3: Alignment parameters corresponding validtion of sensor 5.10.3

6.2.4 Sensor 5.10.4

Studies of planar properties of the sensor 5.10.4 provide an illustration of the applied procedure's ability to detect shift in direction of the *w* axis as well as surface deformation parametrized by parameter P_{11}.

In order to make this method more time-efficient, a threshold limit can be set to value of monitoring tool error. That means no parameters with value less than the monitoring tool error would be accounted for in the alignment procedure. As can be seen from absolute values of corresponding parameters in Table 6.4, deformations would still be detectable in case of sensor 5.10.4.

However, besides the main already mentioned deformations, some other parameter values (e.g. P_{12}) are comparable with the monitoring tool error values. This makes them relevant for future analysis and minimization procedure.

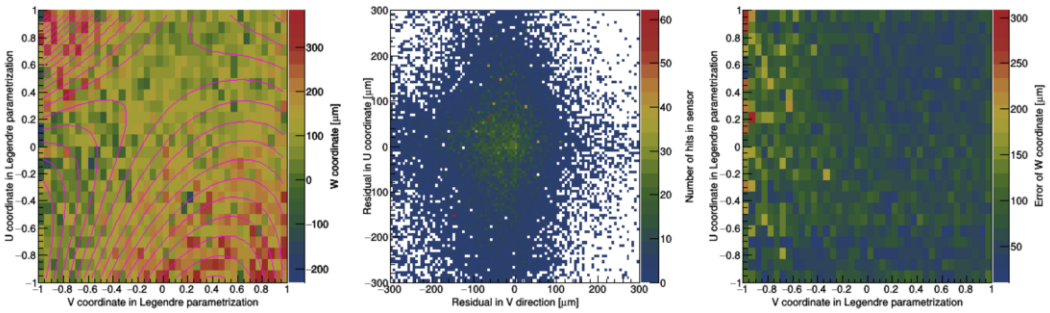

Figure 6.18: Validation plots of sensor 5.10.4

Parameter	$[\mu m]$	*Parameter*	$[\mu m]$
P_U	-4.25 ± 0.77	P_V	-45.27 ± 0.60
P_W	69.70 ± 0.28	P_{20}	24.04 ± 0.62
P_α	25.21 ± 0.46	P_{03}	-12.49 ± 0.67
P_β	-22.47 ± 0.51	P_{12}	51.53 ± 1.13
P_{02}	-10.48 ± 0.58	P_{21}	-34.20 ± 1.09
P_{11}	-81.73 ± 0.83	P_{30}	5.19 ± 0.68
Monitoring tool error			59.44

Table 6.4: Alignnent parameters obtained by the validation procedure for sensor 5.10.4

6.2.5 Sensor 6.12.3

Another example of spatial shifts and rotations can be demonstrated by Figure 6.19 showing validation procedure results for sensor 6.12.3. Large shift in the direction of the u axis is observable from the residual distribution and indicated by the magnitude of P_U parameter value in Table 6.5. This method also successfuly detected rotation corresponding to angle β. Both of the corresponding parameter values, P_U and P_β, are larger than the monitoring tool error and therefore significantly affect detector tracking precision.

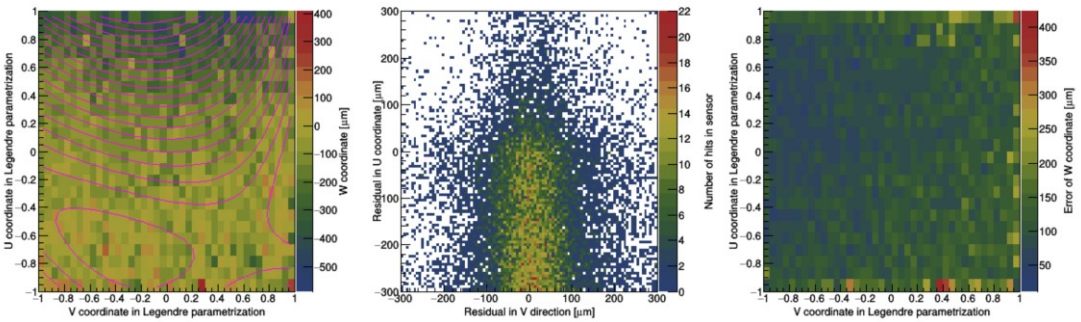

Figure 6.19: Validation plots of sensor 6.12.3 demonstrating shift in the *u* direction and planar deformations of the sensor

Parameter	$[\mu m]$	*Parameter*	$[\mu m]$
P_U	-106.80 ± 0.91	P_V	12.01 ± 0.65
P_W	-71.87 ± 0.28	P_{20}	-56.18 ± 0.61
P_α	18.19 ± 0.43	P_{03}	10.27 ± 0.50
P_β	-114.84 ± 0.55	P_{12}	65.23 ± 0.98
P_{02}	37.25 ± 0.53	P_{21}	16.84 ± 0.88
P_{11}	35.96 ± 0.83	P_{30}	6.99 ± 0.58
Monitoring tool error			95.27

Table 6.5: Alignment parameters corresponding to validation of sensor 6.12.3

6.2.6 Rate of reconstructed cosmic tracks

Rate of reconstructed cosmic tracks for the entire VXD detector reached 5.26 s^{-1}, the rate corresponding to separate parts was slightly lower - for the strip part only the rate of 5.01 s^{-1} was detected, while for the PXD and SVD rate of reconstructed trajectories detected in both parts was only as low as 0.25 s^{-1}. Nice correspondence can be seen when comparing this data with previous results (shown in Figure 6.9). Small discrepancy can be explained by application of more constrining cuts and better alignment corrections.

7 Discussion

The main objective of this thesis was focused on quality monitoring of the vertex detector alignment. The author's analysis consisted of two separate parts, each of which dealt with a different alignment validation method.

In the first part of this work, five different cosmic rays datasets were analyzed. These sets corresponded to a result of quality monitoring procedure for initial detector geometry and four iteratively aligned detector geometries. Each iteration of the alignment procedure applied additional corrections to previous sensor positions.

Cosmic data served as a useful tool for monitoring of alignment quality. The low tendency of cosmic particles, mostly muons, to interact with material of the detector allows these particle traverse through the entire volume of the detector. That helps with connecting signals detected in two separate opposing detector half-shells. Another advantage of working with cosmic ray particles is the possibility to perform the alignment procedure once the detector body is assembled before the detector is brought into service.

Basic characteristics of reconstructed tracks dependent on alignment parameters were visualized by methods of Root software toolkit. These reconstructed track properties included, for example, number of hits per track, number of hits per layer and χ^2 / number of degrees of freedom. Comparison of each one of these quantities for all the datasets available, including all the recorded tracks into the statistics, provided supporting evidence for alignment progress. Track based alignment method was successfully capable of determining values of alignment parameters corresponding to shifts along the local sensor coordinate axes and rotations around these axes respectively. When treating each sensor as a rigid body object, its spatial position was described by 6 degrees of freedom which were fully determined by this alignment monitoring method.

Results obtained in the first section were comparable with the predictions made by Monte Carlo studies after only four iterations of the alignment procedure. Slightly better agreement could be achieved with more repetitions of the iterative process.

The final stage of detector installation is expected to bring significant precision improvement. Precision will also be enhanced by combining the analyzed data with the measurements made by the central drift chamber. The plan is to also incorporate

measurements which account for the presence of magnetic field. This could improve tracking abilities of the detector and lead to higher accuracy of particle momentum calculations. With the start of commissioning runs and beam data collecting, the alignment procedure will be carried out with use of diverse trajectory datasets.

The second part of the thesis introduced and tested new alignment monitoring method. The improvement in tracking quality observed in the first section was significant, however, keeping in mind the desired precision level, not satisfactory. Elaborating on this thesis consultant's idea of applying Legendre parametrization to the planarity plots of surface deformations, new possibilities to ameliorate alignment procedure quality arose. Fitting planarity validation plots by a function constructed of Legendre polynomials of different orders turned out to be an effective tool in revealing planar deformations of sensors and therefore allowed for determination of additional alignment parameters. With the use of corrections to planar deformations the final resulting sensors characteristics resembled characteristic similar to the Monte Carlo model. The biggest drawback of this method is its incapability to detect rotation about the w coordinate axis indicated by the P_γ parameter. Analysis of validation plot histograms is successful in detecting rigid body parameter changes and deviations. In order to estimate remaining surface deformations, fitting of other alignment parameters is necessary.

The most significant advantage of this method is the possibility of its easy application in online monitoring. After each run, the procedure can be easily carried out and is capable of alerting the alignment expert to the need of alignment procedure application. Numerical values obtained as a result of this method are not precise enough to be directly used as geometry corrections. However, they can reliably indicate the magnitude of the displacement.

8 Conclusion

In this thesis, results of the alignment procedure applied to cosmic data collected by the full Belle II vertex detector are presented. Cosmic tracks used for this analysis were collected during the VXD Commissioning run within the time period spanning from October to November 2018. The results are based on application of monitoring and validation tools during alignment studies.

First part of the thesis was dedicated to introduction of the Belle II detector. Functions of its individual components as well as the principles of their mutual cooperation were discussed. Besides the vertex detection system, the reconstruction software, trigger system and data acquisition system used during VXD commissioning data taking were described.

The second part of the thesis explained individual steps of the alignment procedure. Presented illustrations and descriptions focused on algorithms, such as general alignment algorithm and Millepede II, used for alignment studies. Monitoring and validation tools were described in detail. Monte Carlo studies provided illustrative description of effects of initial misalignment and displacements on validation tools.

Cosmic ray data, especially muons, served as a valuable tool for quality evaluation of alignment procedure results because of their low cross section resulting in their ability to pass through the entire detector body volume. In this section, several combinations of obtained alignment parameters were monitored and validated using the same sample dataset. Tracking properties of reconstructed muon trajectories were compared and analyzed.

The latter part of the thesis focused on explanation of differences between rigid body and surface deformation parameters. A new tool for determination of many alignment parameters from vertex detector validation tools is introduced. This tool is effective not only for rigid body parameters determination but also for identification of sensor surface deformations using Legendre polynomials.

The sensitivity and usefulness of this method was illustrated using results of its application on several selected sensors.

Bibliography

[1] KANDRA, J., 2016, *Simulation of Belle II physics events and performance tests of reconstruction.* Master thesis.

[2] DOLEŽAL Z., S. UNO et al. Belle II Technical Design Report. 1 Nov 2010, arxiv: 1011.0352v1 [physics.ins-det].

[3] BILKA, T., 2014, *Simulation and analysis of tests of Belle II vertex detector sensors.* Master thesis.

[4] HIGH ENERGY ACCELERATOR RESEARCH ORGANIZATION, KEK, A Search for New Physics - The Belle II Experiment, 2014. YouTube [online], [Accessed 12 April 2019]. https://youtu.be/nGCrrgXSEOk

[5] MARINAS, C. and VOS, M., 2011, The Belle-II DEPFET pixel detector: A step forward in vertexing in the superKEKB flavour factory. *Nuclear Instruments and Methods in Physics Research Section A: Accelerators, Spectrometers, Detectors and Associated Equipment*. 2011. Vol. 650, no. 1p. 59–63. DOI 10.1016/j.nima.2010.12.116.

[6] SCHIECK, J., 2013, DEPFET pixels as a vertex detector for the Belle II experiment. *Nuclear Instruments and Methods in Physics Research Section A: Accelerators, Spectrometers, Detectors and Associated Equipment.* 2013. Vol. 732, p. 160–163. DOI 10.1016/j.nima.2013.05.054.

[7] KANDRA, J. and BILKA, T., 2017, Alignment and physics performance of the Belle II vertex detector. *Proceedings of The 15th International Conference on Flavor Physics & CP Violation — PoS(FPCP2017)*. 2017. DOI 10.22323/1.304.0053.

[8] KANDRA, J. : Private communication.

[9] Trigger (particle physics), 2018. *Wikipedia* [online], [Accessed 15 April 2019]. https://en.wikipedia.org/wiki/Trigger_(particle_physics)

[10] LIBRETEXTS, 2019, 11.3: Motion of a Charged Particle in a Magnetic Field. Physics *LibreTexts* [online]. 2 May 2019. [Accessed 24 April 2019]. https://phys.libretexts.org/Bookshelves/University_Physics/Book:_University_Physics_(OpenStax)/Map:_University_Physics_II_-_Thermodynamics,_Electricity,_and_Magnetism_(OpenStax)/11:_Magnetic_Forces_and_Fields/11.3:_Motion_of_a_Charged_Particle_in_a_Magnetic_Field

[11] ALISON, JOHN, 2013, Detector Alignment. *CERN Document Server* [online]. 28 March 2013. [Accessed 15 April 2019]. https://cds.cern.ch/record/1536507

[12] BLOBEL, VOLKER, KLEINWORT, CLAUS, 2002, A New Method for the High-Precision Alignment of Track Detectors. *arXiv.org* [online]. 16 August 2002. [Accessed 2 April 2019]. https://arxiv.org/abs/hep-ex/0208021

[13] BILKA, T and KANDRA, J, 2018, Calibration and Alignment Framework for the Belle II detector. *Journal of Physics: Conference Series*. 2018. Vol. 1085, p. 032023. DOI 10.1088/1742-6596/1085/3/032023.

[14] BEKTASOGLU, M. and ARSLAN, H., 2013, Investigation of the zenith angle dependence of cosmic-ray muons at sea level. *Pramana*. 2013. Vol. 80, no. 5p. 837–846. DOI 10.1007/s12043-013-0519-2.

[15] BEATTY, J.J,MATTHEWS, J. S.P. WAKELY,S.P., 2015, *Cosmic Rays*

[16] GAISSER, T. K., ENGEL, R. and RESCONI, E.,Cosmic Rays and Particle Physics by Thomas K. Gaisser. *Cambridge Core* [online]. [Accessed 7 May 2019]. https://www.cambridge.org/core/books/cosmic-rays-and-particle-physics/C81BA71195ADFC89EFCC2C565B617702

[17] GRIEDER, P.K.F, 2008, *Cosmic rays at earth: researchers reference manual and data book*. Amsterdam : Elsevier.

[18] "Atmospheric Interactions." *The Cosmic Connection,* cosmic.lbl.gov/SKliewer/Cosmic_Rays/Atmosphere.htm.

[19] MITTAL, V. K. ,VERMA, R. C. , GUPTA, S. C, 2018, Introduction to nuclear and particle physics. Delhi : PHI LEARNING.

[20] BEETJEDWARS. [Accessed 7 April 2019]. http://upload.wikimedia.org/wikipedia/commons/2/2c/AirShower.svg under GNU Free Documentation License, March 2008.

List of Figures